The Brazilian Global Atmospheric Model (BAM): Performance for Tropical Rainfall Forecasting and Sensitivity to Convective Scheme and Horizontal Resolution

SILVIO N. FIGUEROA,[a,b] JOSÉ P. BONATTI,[a] PAULO Y. KUBOTA,[a,b] GEORG A. GRELL,[c] HUGH MORRISON,[d] SAULO R. M. BARROS,[e] JULIO P. R. FERNANDEZ,[a] ENVER RAMIREZ,[a] LEO SIQUEIRA,[f] GRAZIELA LUZIA,[a] JOSIANE SILVA,[a] JULIANA R. SILVA,[a] JAYANT PENDHARKAR,[a,b] VINICIUS B. CAPISTRANO,[a,b] DÉBORA S. ALVIM,[a,b] DIEGO P. ENORÉ,[a] FÁBIO L. R. DINIZ,[a] PRAKI SATYAMURTI,[g] IRACEMA F. A. CAVALCANTI,[a] PAULO NOBRE,[a,b] HENRIQUE M. J. BARBOSA,[h] CELSO L. MENDES,[g] AND JAIRO PANETTA[i]

[a] *Center for Weather Forecasting and Climate Studies, National Institute for Space Research, Cachoeira Paulista, São Paulo, Brazil*
[b] *Brazilian Research Network on Global Climate Change (Rede CLIMA), São José dos Campos, São Paulo, Brazil*
[c] *National Oceanic and Atmospheric Administration/Earth System Research Laboratory, Boulder, Colorado*
[d] *National Center for Atmospheric Research,[j] Boulder, Colorado*
[e] *Department of Applied Mathematics, University of São Paulo, São Paulo, Brazil*
[f] *Rosenstiel School of Marine and Atmospheric Science, University of Miami, Miami, Florida*
[g] *National Institute for Space Research, São José dos Campos, São Paulo, Brazil*
[h] *Department of Physics, University of São Paulo, São Paulo, Brazil*
[i] *Technological Institute of Aeronautics (ITA), São José dos Campos, São Paulo, Brazil*

(Manuscript received 1 April 2016, in final form 19 July 2016)

ABSTRACT

This article describes the main features of the Brazilian Global Atmospheric Model (BAM), analyses of its performance for tropical rainfall forecasting, and its sensitivity to convective scheme and horizontal resolution. BAM is the new global atmospheric model of the Center for Weather Forecasting and Climate Research [Centro de Previsão de Tempo e Estudos Climáticos (CPTEC)], which includes a new dynamical core and state-of-the-art parameterization schemes. BAM's dynamical core incorporates a monotonic two-time-level semi-Lagrangian scheme, which is carried out completely on the model grid for the tridimensional transport of moisture, microphysical prognostic variables, and tracers. The performance of the quantitative precipitation forecasts (QPFs) from two convective schemes, the Grell–Dévényi (GD) scheme and its modified version (GDM), and two different horizontal resolutions are evaluated against the daily TRMM Multisatellite Precipitation Analysis over different tropical regions. Three main results are 1) the QPF skill was improved substantially with GDM in comparison to GD; 2) the increase in the horizontal resolution without any ad hoc tuning improves the variance of precipitation over continents with complex orography, such as Africa and South America, whereas over oceans there are no significant differences; and 3) the systematic errors (dry or wet biases) remain virtually unchanged for 5-day forecasts. Despite improvements in the tropical precipitation forecasts, especially over southeastern Brazil, dry biases over the Amazon and La Plata remain in BAM. Improving the precipitation forecasts over these regions remains a challenge for the future development of the model to be used not only for numerical weather prediction over South America but also for global climate simulations.

1. Introduction

Substantial progress has been made during the last decade in the development of Earth system models (ESMs) and in the simulation of many important features of the present global climate. Nevertheless, most current models still have serious deficiencies in simulating the tropical precipitation during the wet season over

[j] The National Center for Atmospheric Research is sponsored by the National Science Foundation.

Corresponding author address: Silvio N. Figueroa, CPTEC/INPE, Rod Presidente Dutra, km 40, Cachoeira Paulista, São Paulo, CEP 12.360-000, Brazil.
E-mail: nilo.figueroa@inpe.br

DOI: 10.1175/WAF-D-16-0062.1

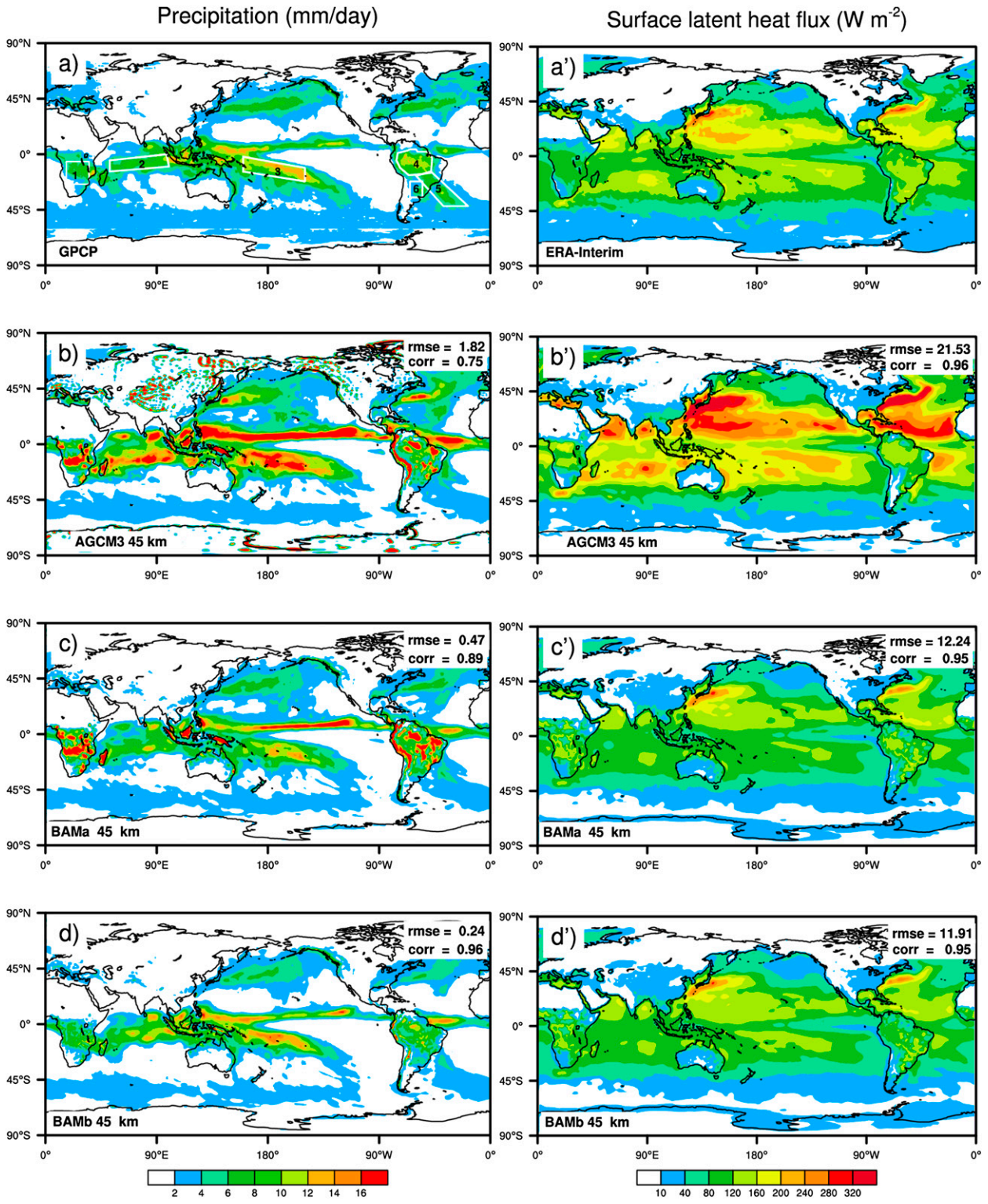

FIG. 1. (left) Precipitation and (right) surface latent heat fluxes averaged over DJF 2012/13 from (a) GPCP, (a′) ERA-Interim reanalysis, and the 24-h forecast of the models. (b),(b′) Old model AGCM3 (Exp1), (c),(c′) new model BAMa (Exp2), and (d),(d′) new model BAMb with GDM convective scheme (Exp3). Model identifications are indicated in the bottom-left corner of the panels, while spatially averaged RMSE and correlation coefficient (CORR) are given in the top-right corner of the panels. Boxes defined in (a) indicate approximately the regions with intense precipitation during DJF over the Southern Hemisphere. Africa (1), the Indian Ocean ITCZ (2), the SPCZ (3), the Amazon basin (4), the SACZ (5), and the La Plata basin (6).

the Southern Hemisphere [December–February (DJF)]. The largest errors are found over the six regions depicted in Fig. 1a: central Africa, the Indian Ocean intertropical convergence zone (ITCZ), the South Pacific convergence zone (SPCZ), the Amazon basin, the South Atlantic convergence zone (SACZ), and the La Plata basin. For instance, results from the Coupled Model Intercomparison Project phase 5 (CMIP5) show that most models tend to underestimate rainfall over the Amazon basin (e.g., Yin et al. 2013; Mehran et al. 2014; Gulizia and Camilloni 2014) and exhibit persistent errors in simulating the South American monsoon system (SAMS; Jones and Carvalho 2013). Over Africa and Australia, models also show poor skill in precipitation simulation (Mehran et al. 2014), and the SPCZ is still poorly simulated in CMIP5 models (Hirota and Takayabu 2013; Grose et al. 2014). Moreover, as rainfall is a highly nonlinear phenomenon, it is difficult to trace back the origin of errors by using full Earth system models.

Xie et al. (2012) and Ma et al. (2014) examined the correspondence between short- and long-term systematic errors in atmospheric models and found that most of the systematic errors in precipitation from climate simulations develop within the first few days (~5 days) of simulation. Therefore, it is believed that improving quantitative precipitation forecasts (QPF) in short-time integrations (1–7 days), for instance, may be useful for improving climate variability simulations. With this perspective, the Brazilian Global Atmospheric Model (BAM) has been developed at the Center for Weather Forecasting and Climate Studies [Centro de Previsão de Tempo e Estudos Climáticos (CPTEC)] of the National Institute for Space Research [Instituto Nacional de Pesquisas Espaciais (INPE)] for use in time scales ranging from days to seasons and at horizontal resolutions O(10–200) km. The strategy was to develop a seamless framework for weather/climate prediction. Hence, the same global atmospheric model used in deterministic NWP (1–10 days) or, coupled to an ocean model, in probabilistic extended NWP (1–4 weeks) is designed to be used also in full ESMs (global coupled atmosphere–ocean–land–cryosphere) for seasonal climate prediction and climate change studies.

A comprehensive performance analysis of the BAM model in NWP and climate predictions is yet to be documented. The present work is focused on evaluating 7-day tropical precipitation forecasts produced by BAM during the austral summer (DJF) of 2012/13 over the Southern Hemisphere, against the daily Tropical Rainfall Measuring Mission (TRMM) and Multisatellite Precipitation Analysis (TMPA). The aim of this paper is to provide 1) a brief description of the dynamical and physical processes in BAM; 2) a QPF skill evaluation of the new model with two different convective parameterization schemes—the Grell and Dévényi (2002) ensemble scheme (GD) and its modified version (GDM) developed at CPTEC against the TMPA dataset; and 3) an evaluation of the impact of increased horizontal resolution (from 45 to 20 km) on the QPF skill. Although the importance of other physical processes such as radiation, vertical diffusion, microphysics, and surface processes for tropical precipitation cannot be overlooked, our main focus lies on deep convection, which is crucial for rainfall prediction (Fritsch and Carbone 2004), and on the impact of increasing horizontal resolution on precipitation forecasts.

Although this study evaluates the performance of the model over all the tropics, our attention lies mainly on southeastern Brazil, where the maximum seasonal precipitation occurs during DJF, and where large metropolitan areas (e.g., São Paulo, Rio de Janeiro, and Belo Horizonte) rely on precipitation for water supply and food production. Therefore, development of a stable global atmospheric model and its validation are important for practical use in weather forecasting over Brazil, as well as the atmospheric component of the Brazilian Earth System Model (BESM; Nobre et al. 2013) for seasonal climate prediction and climate change studies. Hence, the importance of this study is to identify strengths and weaknesses of BAM for its use as an operational NWP model and for further developments of the model. This paper is organized as follows. In section 2, the physics and dynamics formulations of the new model are briefly described. Section 3 describes the design of the experiments, precipitation dataset, and methodology used. Evaluation of the QPF over the tropical region with two different convective schemes and the evaluation of the impact of increased horizontal resolution on the QPF skill are described in section 4. Section 5 summarizes our results.

2. Overview of model formulation

The dynamical core and physics parameterizations in BAM are quite different from those used in the previous CPTEC atmospheric global model (referred to hereafter as AGCM3 or as the old model). We describe here briefly the novelties and the motivations leading to the development of the new model. The original version of AGCM3 was adapted from the Center for Ocean–Land–Atmosphere Studies (COLA) AGCM during the 1990s (Cavalcanti et al. 2002). The evolution of the CPTEC/COLA AGCM, which led to AGCM3, has been reported upon in, for example, Figueroa et al.

TABLE 1. Summary of the dynamic and physics configurations in AGCM3 and BAM.

Dynamics and physics	CPTEC/AGCM3 (old)	CPTEC/BAM (new)
Dynamics	Spectral EU or SL semi-implicit model, with hydrostatic approximation, sigma vertical coordinates, full or reduced Gaussian grids, fully parallel (MPI + OPenMP)	Spectral EU or SL semi-implicit model, with hydrostatic approximation, sigma/hybrid vertical coordinates, full or reduced Gaussian grids, SL monotonic transport scheme (on the model grid) of moisture, microphysics prognostic variables and tracers, fully parallel (MPI + OPenMP)
Land surface processes	Simplified Simple Biosphere Model (SSiB; Xue et al. 1991)	Dynamic vegetation model, IBIS (Foley et al. 1996; Kucharik et al. 2000), implemented, adapted, and improved by Kubota (2012)
Sea–air surface fluxes	The bulk transfer coefficients are determined by analytical functions (Sato et al. 1989)	Bulk transfer coefficients are determined by using Monin–Obukhov theory and the Tropical Ocean and Global Atmosphere Coupled Ocean–Atmosphere Response Experiment (TOGA COARE) dataset (Zeng et al. 1998)
Vertical diffusion	Local Mellor and Yamada (1982), coupled to SSiB equations	Modified Mellor and Yamada (1982) scheme with the addition of the countergradient adjustment term to the eddy diffusion equation
Gravity wave drag	Alpert et al. (1988) scheme without low-level blocking	Webster et al. (2003) scheme with low-level blocking
Cloud microphysics	Single-moment microphysics scheme (Rasch and Kristjansson 1998)	Double-moment microphysics scheme (Morrison et al. 2009)
SW and LW radiation	CLIRAD; Chou and Suarez (1999) and modified by Tarasova and Fomin (2000)	RRTMG; Iacono et al. (2008), developed at AER
Shallow convection	Tiedtke (1983) diffusion scheme	UW shallow convection (Park and Bretherton 2009)
Deep convection	GD	GD and GDM, described briefly in this paper (see the appendix).

(2006), Panetta et al. (2007), and Barbosa et al. (2008) (see Table 1 for a summary). AGCM3 has been extensively used in previous years for deterministic and probabilistic global operational NWP (e.g., Cunningham et al. 2014), and has been coupled to an ocean model for seasonal climate prediction and climate studies (e.g., Nobre et al. 2009, 2013). Nevertheless, many systematic errors in the NWP and climate simulations were found for horizontal resolutions O(10–100) km, such as an excess of oceanic tropical precipitation, wet biases over the Andes, and spurious precipitation near the mountains at high latitudes, among others factors that will be examined later in this article. These errors motivated the development of a new global atmospheric model, which included a new dynamical core and state-of-the-art parameterization schemes.

a. Dynamics core

The dynamical core in BAM is a hydrostatic semi-implicit spectral model, based on a U–V formulation, with a sigma/hybrid vertical coordinate, incorporating a monotonic two-time-level semi-Lagrangian scheme for the tridimensional transport of moisture, microphysical, and tracer prognostic variables. This transport scheme, which can be used with both the Eulerian and the semi-Lagrangian code options for the dynamics, is carried out on the model grid, with moisture variables having no spectral representation. This dynamical core is designed to be used for weather and climate prediction at horizontal resolutions from 200 down to 10 km. In the following subsections, some physical processes incorporated in BAM are described, and others are listed in Table 1. The documentation of the new model (dynamical core and physics formulations) will be available as a technical report.

b. Surface layer processes

The land surface scheme is the Integrated Biosphere Simulator version 2.6 (IBIS v.2.6), which is described by Foley et al. (1996) and Kucharik et al. (2000), and later improved at CPTEC by Kubota (2012). This scheme is a dynamic global vegetation model, which represents a wide range of processes, including land surface physics, canopy

physiology, plant phenology, vegetation dynamics and competition, and carbon and nutrient cycling. The evaluation studies of this scheme over the Amazon (e.g., Costa et al. 2007; Costa and Pires 2010) and over Northeast Brazil (Cunha et al. 2013) have shown the capability of this scheme to well represent the physical, physiological, and ecological processes occurring in vegetation and soils. Therefore, this scheme coupled to the atmosphere is a useful tool for rain forest, land-use, deforestation, and climate change studies, especially over the Amazon.

c. Cloud microphysics

The double-moment bulk microphysics Morrison scheme (Morrison et al. 2005, 2009) with predicted droplet concentration and coupling with the specified background aerosol/cloud condensation nuclei (CCN) spectra is used. This scheme predicts the mass and number mixing ratios of five hydrometeor categories x: cloud droplets, rain, cloud ice, snow, and graupel. The size distributions are represented by gamma functions: $N_x(D_x) = N_{0x} D_x^{\mu_x} \exp(-\lambda_x D_x)$, where D_x is the particle diameter and N_{0x}, λ_x, and μ_x are the intercept, slope, and shape parameters of the size distribution, respectively. The shape parameter is assumed to be zero ($\mu_x = 0$) for cloud ice and precipitation species. For cloud droplets, μ is calculated as a function of the droplet number concentration following Martin et al. (1994). The slope and intercept parameters are derived from the predicted mass q_x and number N_x mixing ratios and specified μ_x. Equations for the time tendencies of q_x and N_x are similar to those in Morrison et al. (2005), except for graupel, and q_g and N_g are given by Reisner et al. (1998). This scheme is coupled to the turbulent mixing scheme, which provides a subgrid vertical velocity for droplet activation and mixing of the cloud droplet and ice number mixing ratios, as well as to the radiation scheme described in the next section using the predicted cloud droplet and ice effective radii.

d. Radiation and cloud properties

The shortwave (SW) and longwave (LW) radiation scheme used in BAM is the Rapid Radiative Transfer Model for GCMs (RRTMG; Iacono et al. 2008) developed at Atmospheric and Environmental Research, Inc. (AER), which is a modified version of the Rapid Radiative Transfer Model (RRTM; Mlawer et al. 1997). This scheme includes the Monte Carlo independent column approximation (McICA) technique (Pincus et al. 2003), which is an efficient statistical method for subgrid cloud characterization. The RRTMG-SW and RRTMG-LW schemes calculate fluxes and heating rates for the shortwave (14 bands, from 0.2 to 12.2 μm) and longwave (16 bands, from 3.1 to 1.0 μm) radiation, respectively. The effects of gaseous absorption and particle scattering into RRTMG-SW include water vapor, carbon dioxide, ozone, methane, oxygen, nitrogen, clouds, aerosols, and Rayleigh scattering, while the molecular species treated into RRTMG-LW are water vapor, carbon dioxide, ozone, methane, nitrous oxide, oxygen, nitrogen, and the halocarbons CFC11 and CFC12. On the other hand, the cloud properties (cloud optical depth, emissivity, etc.) used in this new model are similar to those used in the NCAR Community Atmosphere Model (CAM 5.0) described by Neale et al. (2012). The aerosol optical properties are specified. The implementation of a dynamic aerosol model in BAM is in progress, and is expected to be available in the next model version.

e. Convection

The shallow convection scheme in BAM is from Park and Bretherton (2009), which was developed at the University of Washington (UW). The cloud-base mass flux is calculated using turbulent kinetic energy (TKE) and convection inhibition energy (CINE), and the entrainment and detrainment into cumulus updrafts are calculated using a buoyance-sorting algorithm. Two deep convection schemes have been implemented in BAM: the multiclosure GD scheme and the modified GDM scheme developed at CPTEC/INPE (which is briefly summarized in the appendix). Below, we briefly describe the GD scheme, focusing on the cloud-base mass flux.

Following Arakawa and Schubert (1974, hereafter AS) the cloud-work function A is the rate of generation of kinetic energy due to work done by buoyancy force B, or an integral measure of the buoyance force with weighing by a normalized mass flux profile η. The change of A can be written as $\partial A(t)/\partial t = [\partial A(t)/\partial t]_{\rm LS} + [\partial A(t)/\partial t]_{\rm CU} m_b$, where the subscripts LS and CU represent changes in the work function due to the effects of the large-scale forcing F and due to the convective clouds K normalized by cloud-base mass flux m_b, respectively. The Grell closure (Grell 1993; G1) makes the AS convective quasi-equilibrium assumption between large-scale forcing and convection. This AS quasi-equilibrium assumption requires that $\partial A(t)/\partial t \ll F$. This means that convective tendencies are fast compared to the net or observed tendency, $\partial A(t)/\partial t \approx 0$; then, m_b in the G1 closure can be calculated as $m_b = -F/K = -[A'(n+1) - A(n)]/K\Delta t$, where A' is the work function calculated with updated (at time step $n+1$) thermodynamics variables ψ^{n+1} after modifications by model tendencies (radiation, surface, and PBL processes and dynamics), A is calculated from thermodynamics variables at the present state ψ^n, and K is calculated as in G1. The GD scheme implemented in BAM uses five different methods to calculate m_b. Three

TABLE 2. Experiment descriptions.

Expt	Quadratic grid horizontal resolution with a reduced Gaussian grid	Time step (s)	Dynamics: model version EU or SL	Physics: model version, except deep convection	Deep convection	Model version, dynamics resolution
Exp1	TQ299 (0.4° ≈ 45 km)	240	AGCM3-EU	AGCM3	GD	AGCM3-EU-45 km
Exp2	TQ299 (0.4° ≈ 45 km)	240	BAMa-EU	BAMa	GD	BAMa-EU-45 km
Exp3	TQ299 (0.4° ≈ 45 km)	240	BAMb-EU	BAMb	GDM	BAMb-EU-45 km
Exp4	TQ666 (0.18° ≈ 20 km)	400	BAMb-SL	BAMb	GDM	BAMb-SL-20 km

are stability closures. First, G1 is described above. Second, for AS, the closure from the GFS physics suite is used, employing climatological cloud work functions instead of calculating A. Third, the Kain–Fritsch (KF) type removes stability over a specified time period (such is used in Kain and Fritsch 1992). Next, the Kuo type uses a Krishnamurti-type closure (Krishnamurti et al. 1983), relating the integrated vertical advection of moisture to m_b. The final closure uses a relationship between low-level omega and m_b (Brown 1979). Three perturbations are then applied for G1, KF_type, Kuo_type, and omega, and four perturbations for AS. These are allowed to interact with nine members from static control (three precipitation efficiencies and three cap strengths), giving a total 144 subgrid members.

3. Experiments, data, and methodology

a. Experimental design

Four experiments have been performed. The first experiment (Exp1) uses AGCM3 and the other three use BAM with two convective parameterizations, GD and GDM, which are referred to as BAMa and BAMb, respectively. Further details are given in Table 2. In the first experiment, global precipitation estimates from AGCM3 and BAM are compared (section 4a). The QPF evaluation over the tropics, the sensitivity of the precipitation forecast from the new model (BAM) with two convective parameterizations (Exp2 and Exp3), and the sensitivity to increasing the horizontal resolutions (Exp4) are evaluated in two parts: first (section 4b), over the global tropics, SPCZ, and over three land regions; and second (section 4c), over Brazil, which was divided into five regions. The experiments at 20-km horizontal resolution were carried out with semi-Lagrangian (SL) and Eulerian (EU) advection schemes, but the results were similar (figures not shown). Therefore, we will focus only on the SL results.

The period of simulation is from 20 November 2012 to 28 February 2013. This period was chosen for the present study because during that specific period (i.e., austral summer) many heavy rainfall events were observed. For instance, during DJF 2012/2013, 13 cold fronts were identified over La Plata and five well-defined SACZ episodes occurred over southeastern Brazil (INPE/CPTEC 2012, 2013a,b). Starting with each new day in that period, the models were integrated for 7 days using the same initial conditions employed in the NCEP/GFS operational model, at 1200 UTC. The 7-day output total precipitation forecast was used for model evaluation. We use the initial conditions from GFS to evaluate the performance of the new dynamic and physical processes involved in BAM, rather than using our own assimilation system, to allow for a clear comparison with precipitation forecasts from GFS. To filter the spurious high-frequency oscillations produced during the first time steps of the forecast due to the unbalanced initial conditions, a diabatic nonlinear normal-mode initialization (NNMI) scheme based on Machenhauer (1977) and Kitade (1983) is used for the first five vertical modes, with a period cutoff of 48 h, and two interactions. In this scheme, the initial tendency of the faster modes is set to zero, and the corresponding fields of these waves are replaced by new balanced fields obtained interactively. This initialization process can alleviate the problem of surface pressure tendency spinup during the first few hours of integration.

b. Data for QPF verification

The daily observed rainfall for the tropical QPF evaluation is derived from TMPA (Huffman et al. 2010) 3B42 version 7, with 3-hourly 0.25° × 0.25° latitude/longitude grid resolution rainfall data for the period December 2012–February 2013. Previous studies have evaluated the TMPA product over different tropical regions, for example, over Australia (Chen et al. 2013) and over the Andes (Ochoa et al. 2014). These studies reveal that the TMPA product shows, in general, a good correspondence with rain gauge datasets. In addition to TMPA, for evaluating the global precipitation and surface latent heat fluxes for DJF 2012/13, the daily Global Precipitation Climatology Project (GPCP version 2.2) 1° × 1° latitude/longitude grid (Huffman et al. 2009) product and the European Centre for Medium-Range Weather Forecasts (ECMWF) interim reanalysis product (ERA-Interim; Dee et al. 2011) are used, respectively. For comparison of QPFs from BAM and other global NWP operational

models, 7-day precipitation forecast data from the operational GFS (September 2012 version, horizontal resolution ≈27 km and with 64 vertical levels) is used, which are available on the NCEP website. Finally, the output precipitation data from all experiments were gridded to the observed data resolution [e.g., tropical model precipitation to the TMPA dataset resolution (0.25°) and global model precipitation to the GPCP dataset resolution (1°)]. For this interpolation, the remapcon utility from the Climate Data Operators (CDO) package is used, which performs first-order conservative remapping.

c. *Methodology and statistics*

For evaluating the QPFs in each region we used standard continuous and categorical statistical measures. The continuous statistics scores used to evaluate the accuracy of different models are the unconditional bias (BIAS), root-mean-square error (RMSE), unbiased root-mean-square error (URMSE), standard deviation σ, and Pearson correlation coefficient R. Following Murphy (1988), the uncentered total RMSE can be decomposed into two components, due to the systematic errors (BIAS) and related to the pattern error (URMSE). The URMSE (once the unconditional biases are removed from the total error) can be interpreted as a measure of nonsystematic model errors as a result of errors in amplitude (σ) and phase (R). We use the Taylor (2001) diagrams to graphically summarize the normalized unbiased RMSE (URMSE*), the normalized standard deviations forecast σ_f^* and the correlation coefficient R_{fo}. This method is also used to compare the performance of models to the observations.

The categorical forecast verification measures used here are the frequency bias score (FBS) and the Gilbert skill score (GSS) also known as the equitable threat score (ETS) (Mesinger and Black 1992). The FBS and GSS are among the different categorical scores recommended by WMO (2009) for assessing the skill of deterministic precipitation forecasts. The threshold values used for plots are similar to those used by Mesinger (2008) except they are in millimeters per day. Four different rainfall categories, based on thresholds of precipitation intensity (in mm day^{-1}), are used in this paper: very light rain (0.1–2.5), light rain (2.6–7.5), moderate rain (7.6–35.5), and heavy rain (>35.6). These four rainfall categories have been adapted from the India Meteorological Department's (IMD) glossary (http://www.imdpune.gov.in/weather_forecasting/glossary.pdf).

4. Results

a. *Global precipitation from AGCM3 and BAM*

In this section we evaluate the 24-h global DJF average precipitation and surface latent heat fluxes from AGCM3 and BAM at 45-km horizontal resolution with two convective parameterizations: GD and GDM. Figure 1 shows the seasonal mean precipitation rate obtained from GPCP and the 24-h model forecasts from the first three experiments (left) and the corresponding surface latent heat fluxes (right). The comparison of surface latent fluxes is included in this section, in order to identify the possible causes of the excessive tropical precipitation in AGCM3. The spatially averaged RMSE and correlation coefficient values are shown in the top right corners of the panels, and the zonal mean precipitation and surface latent heat fluxes corresponding to Fig. 1 are shown in Fig. 2. An eyeball comparison of the results from the old model (Fig. 1b) with the observations (Fig. 1a) clearly shows large spurious precipitation over the mountains at high latitudes (e.g., the Rockies, Himalayas, Greenland, and the Antarctic mountains), and large wet biases over tropical regions, especially over Africa, South America, the SPCZ, and the ITCZs. Large differences over high and low latitudes between the old model and GPCP can be vividly observed in Fig. 2a. These errors in AGCM3 are probably caused by the horizontal diffusion applied to moisture and temperature computed in spectral space along pressure surfaces. The new treatment of moisture in the new dynamic spectral core of BAM with a semi-Lagrangian scheme for horizontal and vertical advection carried out completely in grid-point space eliminated this problem (cf. Fig. 1c with Fig. 1b over the high latitudes). In the new dynamical core, no horizontal diffusion is applied to the moisture, microphysics prognostic variables, and trace constituents. In addition, the semi-Lagrangian advection scheme employs a monotonic quasi-cubic interpolation method, preventing the occurrence of over- or undershootings. In particular, positive quantities remain positive.

Concerning the excessive ocean tropical precipitation present in the old model, which was reduced drastically in BAMa, a comparison of the surface latent heat fluxes over tropical regions (Fig. 1b′) with ERA-Interim (Fig. 1a′) suggests that the origin of this wet bias is probably linked to the errors in the surface fluxes formulation over the oceans. Although the forecast of global precipitation in BAMa is improved (cf. Fig. 1b with Fig. 1c, and visible even more clearly in Fig. 2a) wet biases still remain over the Pacific and Atlantic ITCZs, as well as over Africa and South America. However, in BAMb (with the GDM convective scheme), these errors are reduced substantially (cf. Figs. 1d and 1c) (i.e., the wet biases over the ITCZs, Africa, and South America) are largely reduced. On the other hand, while the surface latent heat fluxes do not change significantly between the

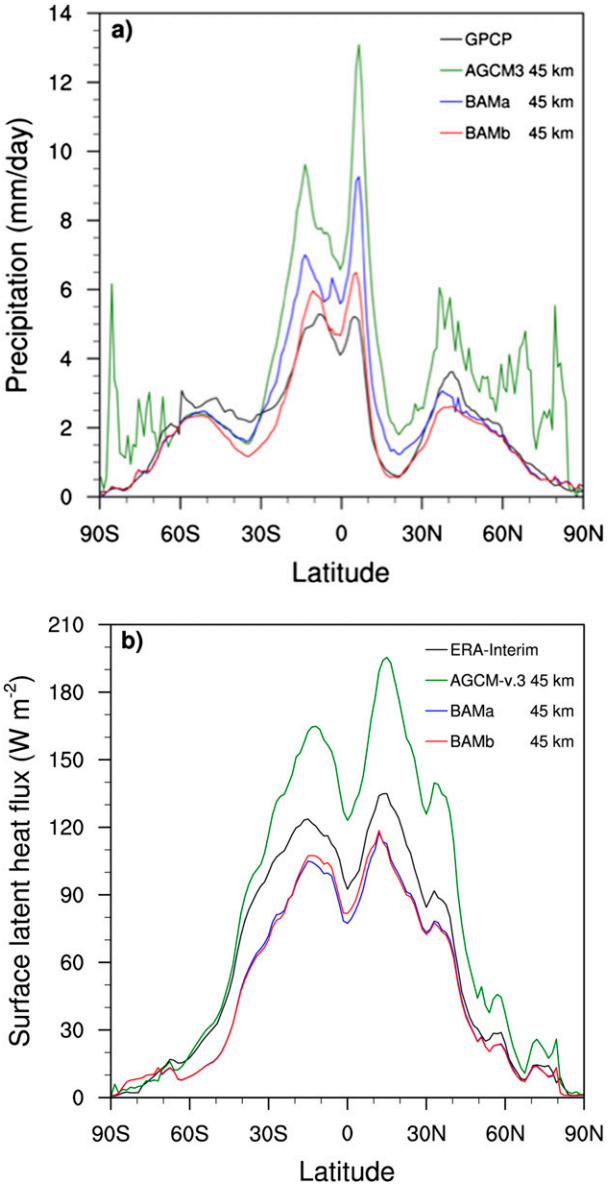

FIG. 2. (a) Zonal mean precipitation and (b) surface latent heat fluxes corresponding to Fig. 1 for 24-h forecasts by the different models indicated in the panels.

BAMa and BAMb zonal averages, they do overcorrect for the excess surface heat flux of AGCM3 (Fig. 2b). The precipitation patterns from 48- and 72-h forecast (figures not shown) are similar to the ones in Figs. 1 and 2. In brief, the GDM scheme in BAM improved the DJF global precipitation compared to the GD scheme and AGCM3, as can be clearly seen in Fig. 2a, yet it is necessary to compare the daily forecast statistics from both convective schemes for 7-day forecasts in order to conclude which convective scheme is better for QPF. In the following sections we will no longer consider AGCM3 for the QPF evaluations; instead, we will mainly focus on the performance of BAM with two convective parameterizations (GD and GDM) and two horizontal resolutions (45 and 20 km) against the observations. Additionally, the performance of BAM is compared with GFS results.

b. *Quantitative precipitation forecast over the tropics*

In this section we focus on the QPF evaluation from Exp2 (45 km), Exp3 (45 km), and Exp4 (20 km) over the tropics and GFS products against daily rainfall data from TMPA. Initially, we analyze the first 24-h forecast mean precipitation (Fig. 3) by comparing the output from BAMb at two horizontal resolutions and GFS against the observed precipitation dataset to illustrate short-term precipitation forecast patterns over the tropics. The left panel in Fig. 3 shows that there are no substantial differences between BAMb at low (Fig. 3b) and high (Fig. 3c) horizontal resolutions and GFS (Fig. 3d) (cf. spatial root-mean-square and the correlation coefficient values), and they appear quite similar to the observations (Fig. 3a). However, in the right panel of Fig. 3, we can identify regions with dry and wet biases. The similarities of the dry and wet biases in all three panels on Fig. 3′ are noteworthy, especially over the mouth of the Amazon River and in the southward anomalous displacement of the Atlantic ITCZ. The main differences between BAMb at low and high resolutions (Figs. 3b′ and 3c′) are observed over Africa and South America with complex topography, where the precipitation forecasts are slightly increased at higher resolution (more details in section 4c), whereas over oceans there are no noticeable differences. In the case of GFS, major errors (overestimation) are found over South America (e.g., the Andes), central Africa, and the tropical and North Pacific Ocean, whereas minor errors are found over the Maritime Continent in comparison to BAM at both resolutions. This visual evaluation over different tropical regions will be analyzed later by their statistical metrics for the 7-day forecast, which will show that the systematic errors over some regions observed in Fig. 3 for the 24-h forecast remain for the next 2–7-day forecast, and over other regions these errors change during 4-day forecast, but remain virtually unchanged for 5–7-day forecasts.

To analyze the QPFs over the tropics, we have chosen five areas shown in Fig. 3a: the global tropics (A1); Africa (A2), northern Australia (A3), and South America (A5), which are tropical continental areas; and SPCZ (A4). Figure 4 displays the time series of precipitation for models and TMPA to help illustrate the daily rainfall forecasts at lead times of 24 and 72 h, and Fig. 5 shows the BIAS (left) and unbiased URMSE (right) for 1–7-day forecast. Figure 4a shows that the precipitation amount over the global tropics for the 24- and 72-h forecasts are

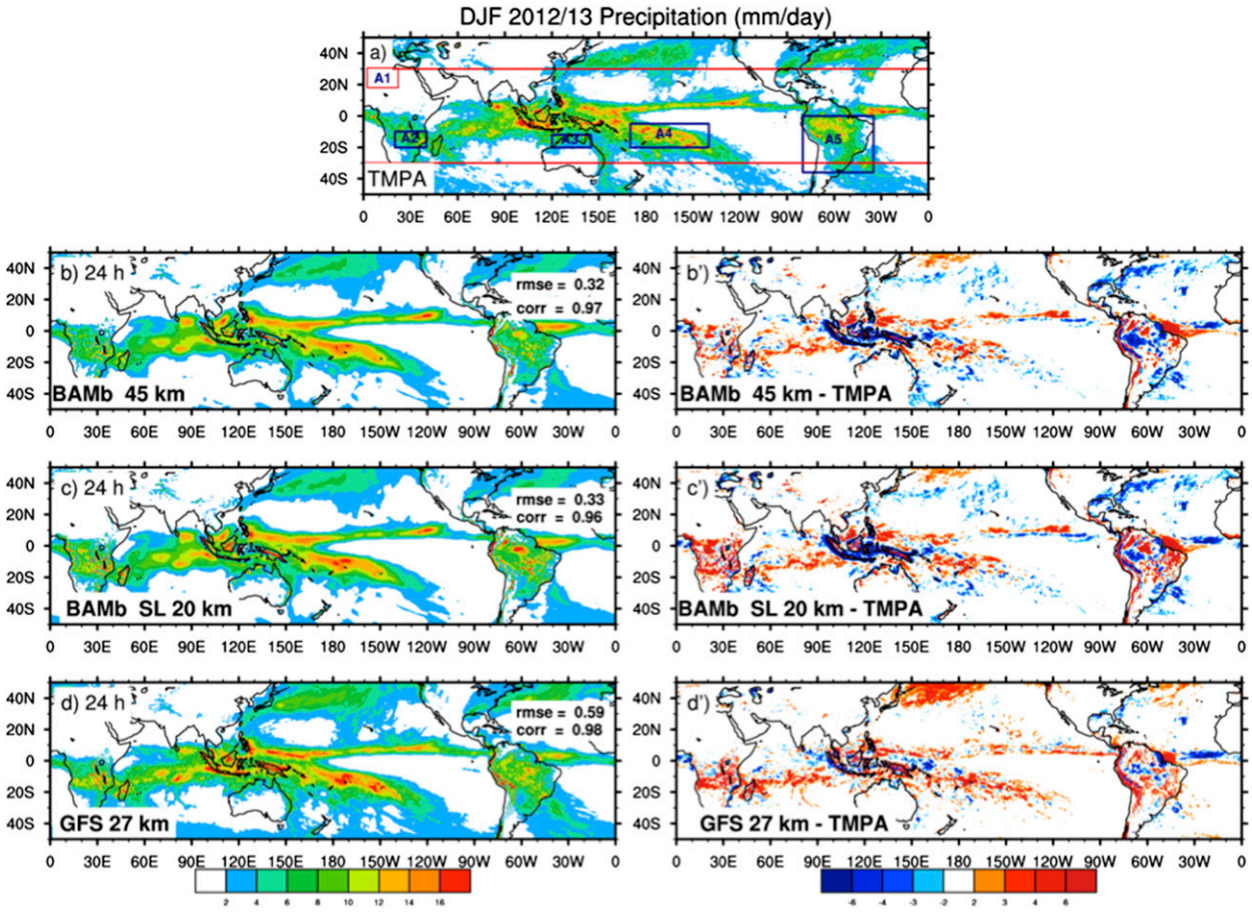

FIG. 3. Mean precipitation averaged over DJF 2012/13 from (a) TMPA-3B4 and from three NWP model 24-h forecasts and their differences from TMPA: (b),(b′) BAMb (Exp3) at 45 km, (c),(c′) BAMb at 20 km (Exp4), and (d),(d′) GFS at 27 km. Rectangular boxes A1, A2, A3, A4, and A5 in (a) are the regions used for the comparison of results: global tropics (30°S–30°N), Africa, Australia, SPCZ, and South America, respectively.

overestimated by BAMa and GFS whereas BAMb shows minor biases, which can be seen clearly in Fig. 5a. This figure also shows that the precipitation bias observed during the first few days remains similar for the medium-range 5–7-day forecasts. The unbiased RMSE analyzed over the global tropics (Fig. 5a′) also shows minimum errors for BAMb compared to GFS and BAMa. The BIAS analysis in specific regions shows (Figs. 4 and 5) that BAMa and GFS overestimate the precipitation over Africa and South America, while BAMb slightly underestimates precipitation. Over Australia and the SPCZ the precipitation biases undergo changes during the first 3-day forecast. Notwithstanding these changes, the precipitation biases for 5–7-day forecasts remain virtually unchanged (e.g., over the SPCZ) or they are enlarged (e.g., GFS and BAMb over Australia). In short, the systematic errors from these models over tropical regions occur within the first 5 days of a forecast. The unbiased RMSE analyzed over different regions shows that BAMa has larger pattern errors than do GFS and BAMb.

The precipitation time series for BAMb at 20-km horizontal resolution (figure not shown) are similar to those for BAMb at 45 km, as shown in Fig. 4, except over Africa and South America, where the model at high resolution increases the precipitation amount (see Figs. 5b and 5e). However, there are no clear differences in RMSE at either resolution. The average dry biases over South America (Fig. 5e) are slightly improved at high horizontal resolution (more details in section 4c).

Figure 6 depicts the GSS along with the FBS of the QPFs with the 72-h forecasts from BAMa, BAMb, and GFS. The frequency bias score is useful for knowing whether the model overpredicted (FBS > 1) or underpredicted (FBS < 1), that is, indicating whether the model predicted either more or fewer events than were observed (it is different from the unconditional bias used before). A perfect score of 1 means that the forecast

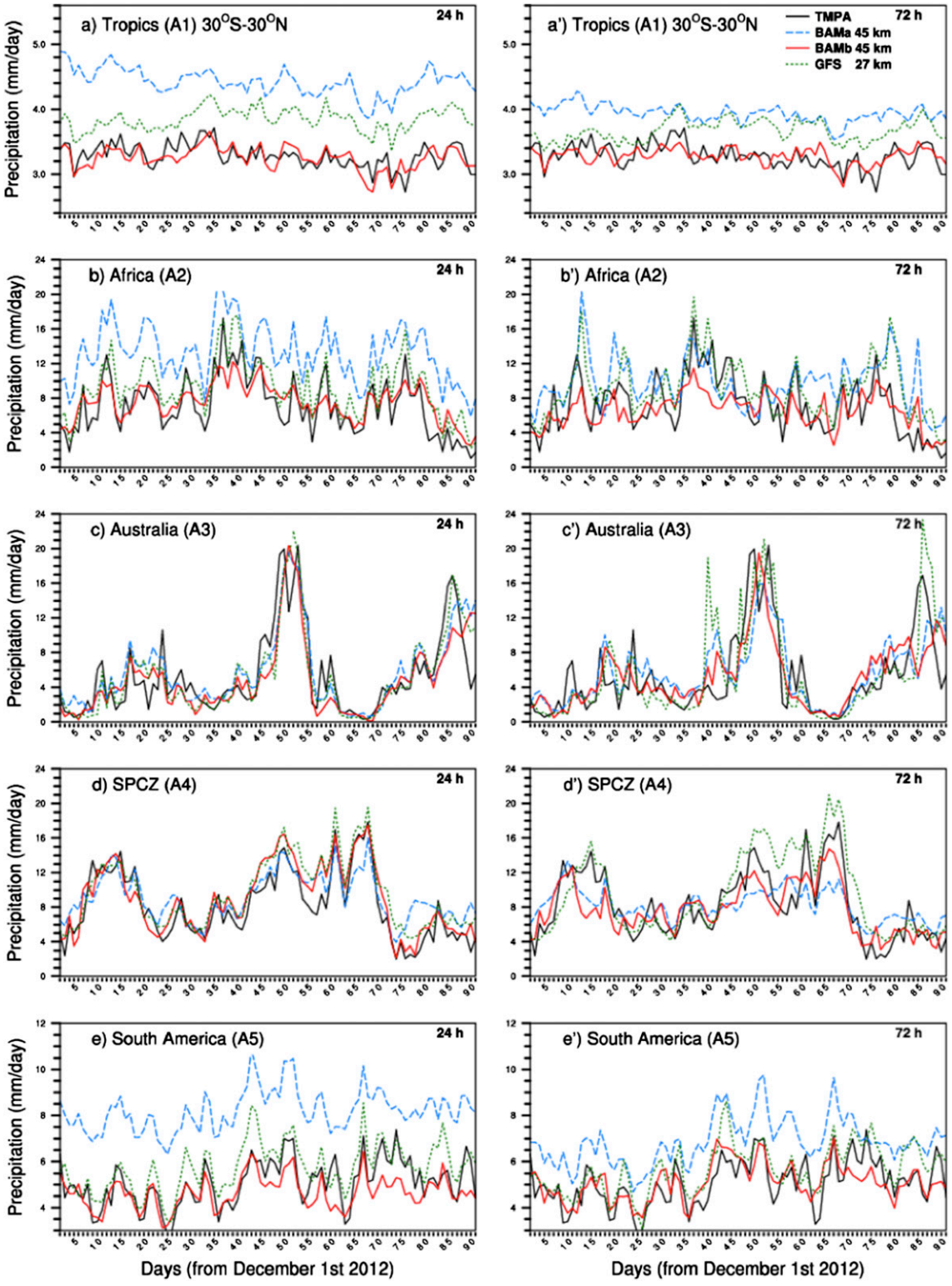

FIG. 4. Daily mean precipitation for the period 1 Dec 2012–28 Feb 2013 from (left) 24- and (right) 72-h forecasts for the areas defined in Fig. 3a from TMPA and three NWP models indicated in the panel.

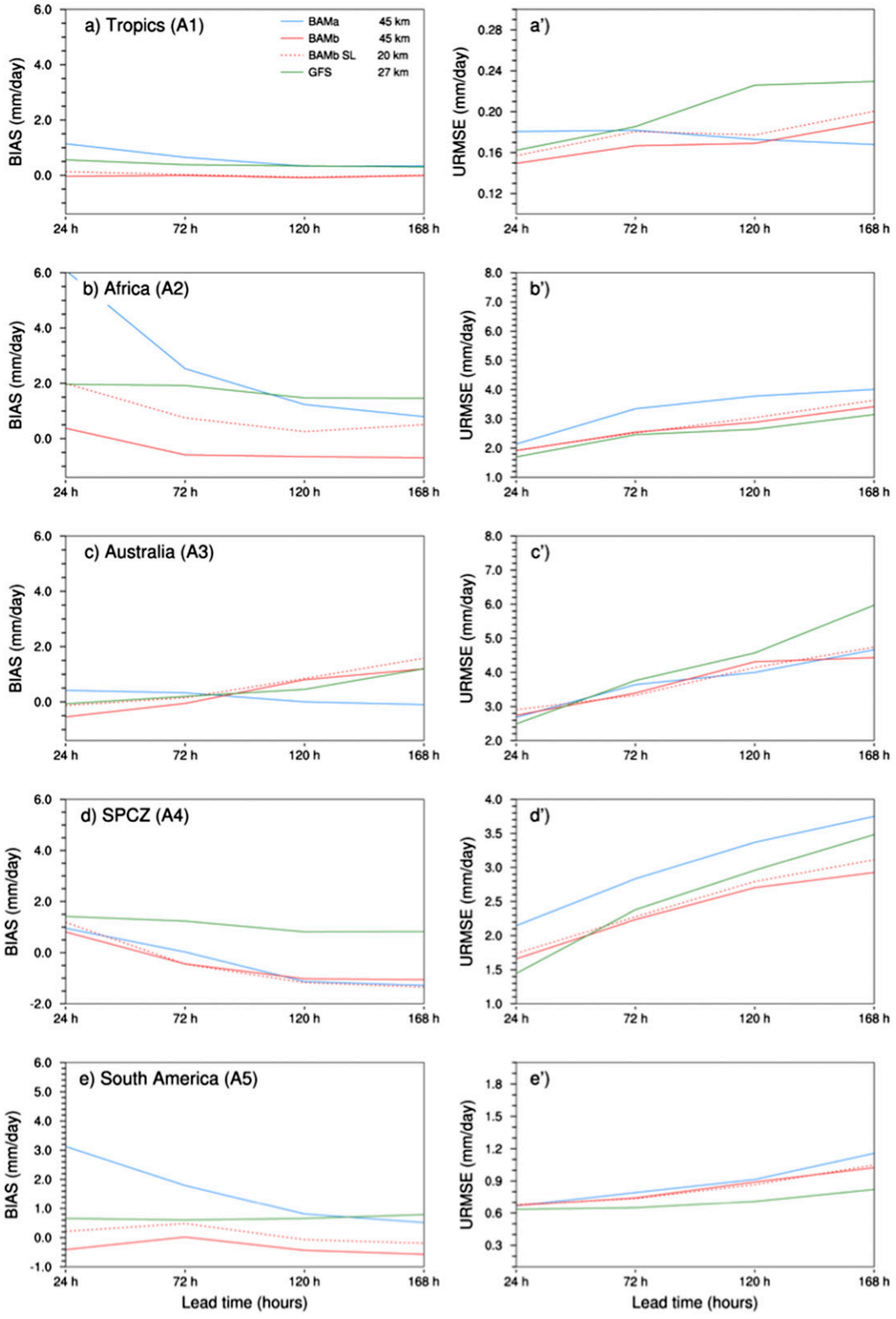

FIG. 5. The performance of the models BAMa (Exp2), BAMb (Exp3 and Exp4), and GFS in terms of precipitation BIAS and URMSE for the areas defined in Fig. 3a.

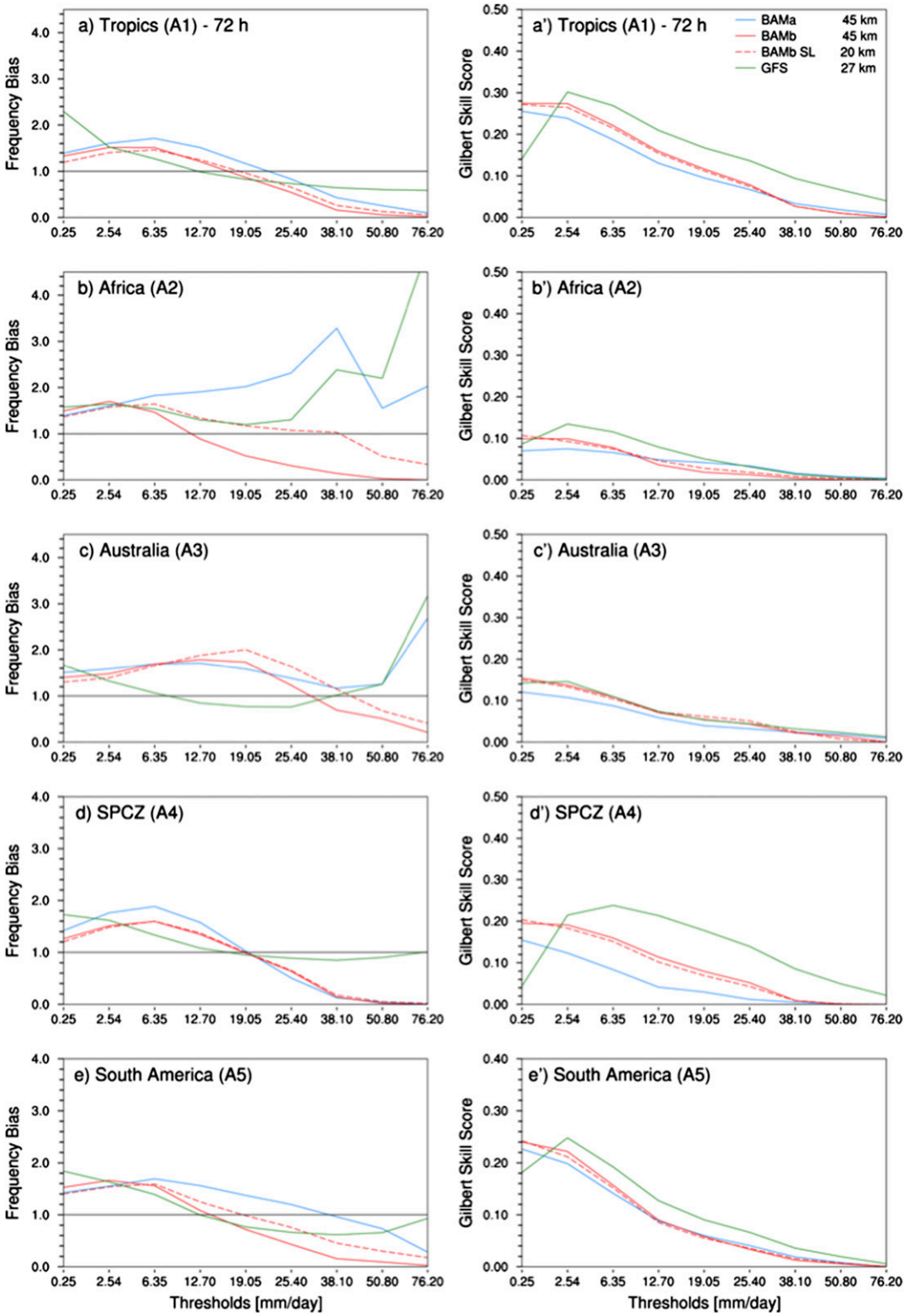

FIG. 6. (left) Frequency bias and (right) GSS as functions of the precipitation threshold for the areas defined in Fig. 3a, 72 h in advance by models indicated in the panel.

frequency is equal to the observed events regardless of forecast accuracy. On the other hand, GSS is commonly used to evaluate the precipitation forecast skill across different regimes, with GSS equal to 0 indicating no skill, 1 indicating a perfect score, and <0 a worse forecast than random. However, this score should be used in combination with FBS (or by adjusting with the bias score), because higher GSS scores can result from FBS results being inflated beyond unity (Mesinger 2008). The analysis of FBS (Figs. 6a–e) and GSS (Figs. 6a′–e′) over the global tropics, as well as over different tropical regions at low resolution, shows that BAMb performs much better than BAMa, with major skill improvement over the SPCZ for light and moderate rainfall. There are no significant differences in GSS scores over all regions as the horizontal resolution is increased. However, a substantial improvement in FBS (values near 1) with increased horizontal resolution for moderate and heavy rainfall over Africa (Fig. 6b) and South America (Fig. 6e) is noted.

To further evaluate the models' performance for amplitude and phase of precipitation patterns over the five areas of study, Taylor diagrams were computed and are shown in Fig. 7. These diagrams allow for the intercomparison of the unbiased RMSE, correlation coefficient, and standard deviation for 1-, 3-, 5-, and 7-day forecasts. In these diagrams, the radial distance (dotted lines) from the origin to any given forecast point indicated by a number (from 1- to 7-day forecasts) is the normalized standard deviations σ_f^* and their cosine of the azimuthal angle related to the horizontal axis gives the correlation coefficients R_{fo}. The distance from the reference point (black star) along the horizontal axis to any given forecast points is in unbiased RMSEs (URSME*), as described in section 3d. Figure 7 shows, first, that BAMb performs better than BAMa over Africa, Australia, South America, and the SPCZ in terms of RMSE, correlations, and the amplitude of spread (standard deviation) with the lead time of 1–7 days remaining consistent with the previous analyses. Second, the results from BAMb at high resolution are similar to the results at low resolution, except over Africa (Fig. 7b) and South America (Fig. 7e), where at 20 km an improvement in the standard deviation is seen. These last results over Africa and South America are consistent with the FBS improvement over these regions (discussed later) and with the improvement in rainfall intensity shown in Fig. 5. We speculate that this improvement, over regions with complex terrain, can be attributed to an improved representation of the topographical forcing in the high-resolution models. It is interesting to see from Figs. 7c and 7d that over Australia and the SPCZ the errors increase (and correlations diminish) as the lead times increase (in both resolutions and especially from 5 to 7 days). Although these results are obtained from an AGCM not coupled to an ocean model, they also indicate that the precipitation predictability for medium-range time scales in some equatorial regions (e.g., Australia and the SPCZ) can be higher than that at high latitudes, as has been suggested by Stern (2008), Zhu et al. (2014), and Stern and Davidson (2015).

In summary, the QPF evaluation from different versions of BAM shows that BAMb at 45 km gives better performance than BAMa (in terms of FBS, GSS, RMSE, BIAS, standard deviation, and correlations) over all of the tropical regions analyzed here. On the other hand, the bias scores of moderate and heavy rain (both for intensity and standard deviation) are improved at high resolution over Africa and South America, which indicates the importance of resolution in improving the representation of extreme precipitation events over these regions. An additional result is that systematic errors (bias) in the model over tropical regions occur within the first 5 days of the forecast.

c. *Quantitative precipitation forecast over Brazil*

To evaluate the performance of BAM for QPFs over Brazil at up to 7 days, we have chosen five regions covering the country, namely, B1, B2, B3, B4, and B5, as shown in Fig. 8. Region B5 includes northern Brazil where the Brazilian Amazon basin (hereafter called the Amazon) is located; region B4 includes most of northeastern Brazil (referred here as the Northeast); region B3 includes central-western Brazil, eastern Bolivia, and northern Paraguay (the Central-West); region B2 includes most of southeastern Brazil and the surrounding oceanic areas (referred to here as the Southeast), where the large Brazilian cities are located (e.g., Rio de Janeiro, São Paulo, and Belo Horizonte); and B1 represents approximately the La Plata basin, which includes most of southern Brazil, Uruguay, northeastern Argentina, and southern Paraguay (hereafter called La Plata).

Before analyzing the QPFs from BAMb, we will review briefly the main features that affect the daily precipitation over regions B1–B5, focusing on the period DJF 2012/13. Figure 9 shows the time series of precipitation for the models and TMPA to illustrate the models' daily precipitation forecasts for 24 h (left) and 72 h (right) over the regions defined in Fig. 8 in comparison to the observations.

The systems that affect the daily precipitation over the La Plata region during DJF are frontal systems (Garreaud and Wallace 1998), mesoscale convective systems (MCSs), and cyclogenesis (e.g., Salio et al. 2007; Romatschke and Houze 2010; Boers et al. 2015;

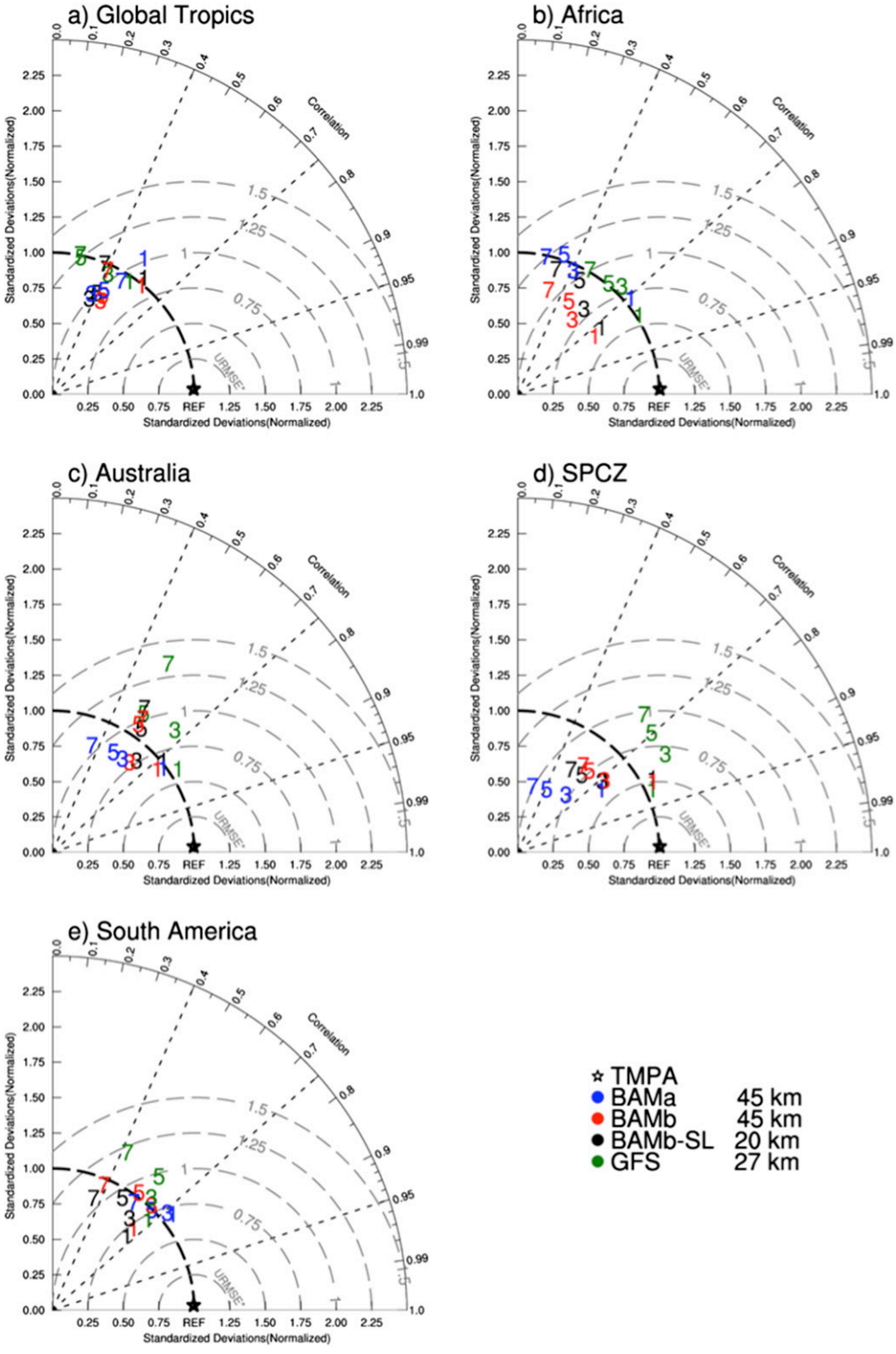

FIG. 7. Taylor diagrams comparing the precipitation simulation statistics, correlation coefficient, URMSE*, and standard deviation normalized from the models for the areas defined in Fig. 3a. The black star indicates perfect agreement. The numbers in the diagram indicate the forecast range (days).

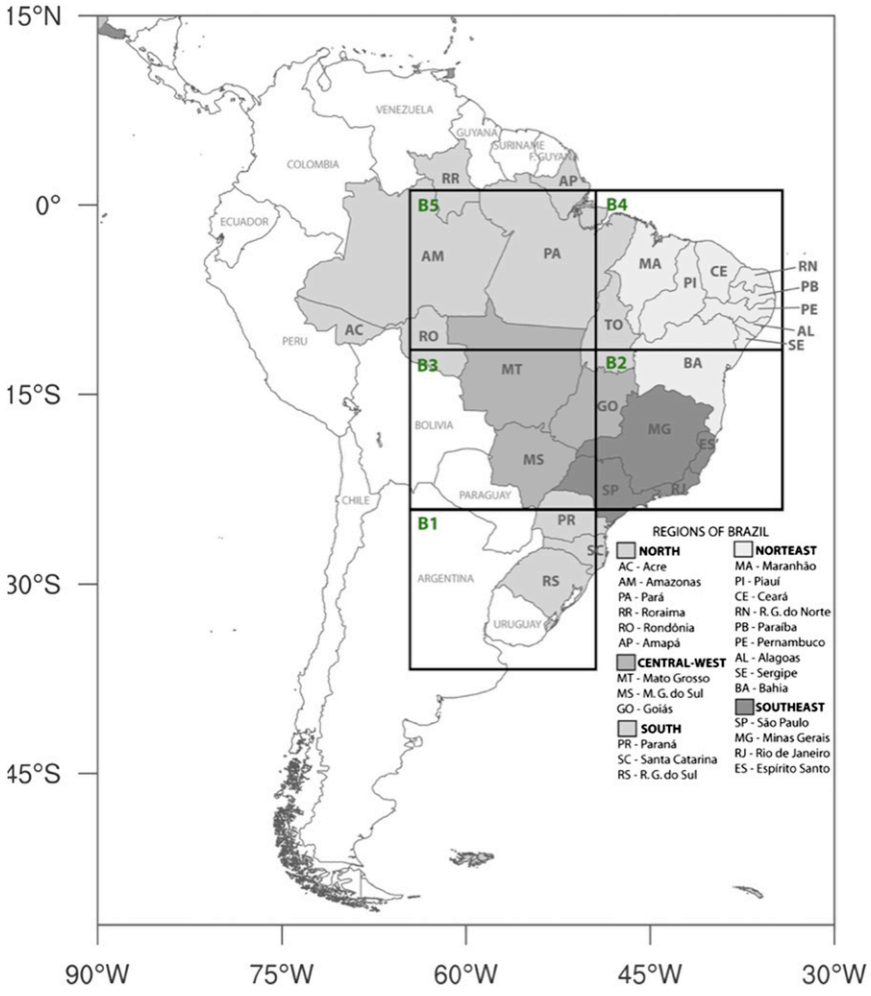

FIG. 8. Map of South America showing the geographic regions of Brazil (shaded). Boxes B1–B5 are considered for model evaluation. B1 represents approximately the La Plata basin (which includes southern Brazil, northeast Argentina, southern Paraguay, and Uruguay). The boxes B2–B5 represent approximately the Southeast, Central West, Northeast, and North regions defined in this paper. B5 also represents approximately the Brazilian Amazon basin (referred to as the Amazon).

Rasmussen et al. 2016). The La Plata basin is a preferred region over southern South America for tropical–extratropical interactions between the large-scale synoptic baroclinic waves (upper-level jet streams and their associated fronts) and warm and moist low-level advection by the low-level jet (LLJ) on the eastern side of the Andes from the Amazon region, generating the majority of the MCSs observed in this region (e.g., Berbery and Barros 2002; Salio et al. 2007; Rozante and Cavalcanti 2008; Arraut and Barbosa 2009; Arraut and Satyamurty 2009; Boers et al. 2014; Rasmussen and Houze 2016). Although the occurrence of some MCSs over this region does not relate to the frontal systems, the most numerous and intense MCSs tend to occur in connection with LLJs and cold fronts passing over the southern Andes and arriving across northern Argentina, Uruguay, and southern Brazil (Romatschke and Houze 2010; Rasmussen and Houze 2016).

During DJF 2012/2013, 13 cold fronts were identified over the region (INPE/CPTEC 2012, 2013a,b), which is indicated by the letter F in Fig. 9a (from F1 to F13), giving an average of a cold front passage every 7 days. We can see that all models forecasted these systems 24 and 48 h in advance, although with different intensities.

Among the main systems that produce rainfall over the Southeast (B2) (e.g., the SACZ, frontal systems, MCSs, squall lines, and land–sea-breeze circulation), the SACZ (a quasi-stationary meteorological perturbation that lasts for 3–7 days, approximately) is the most important among the synoptic systems directly affecting

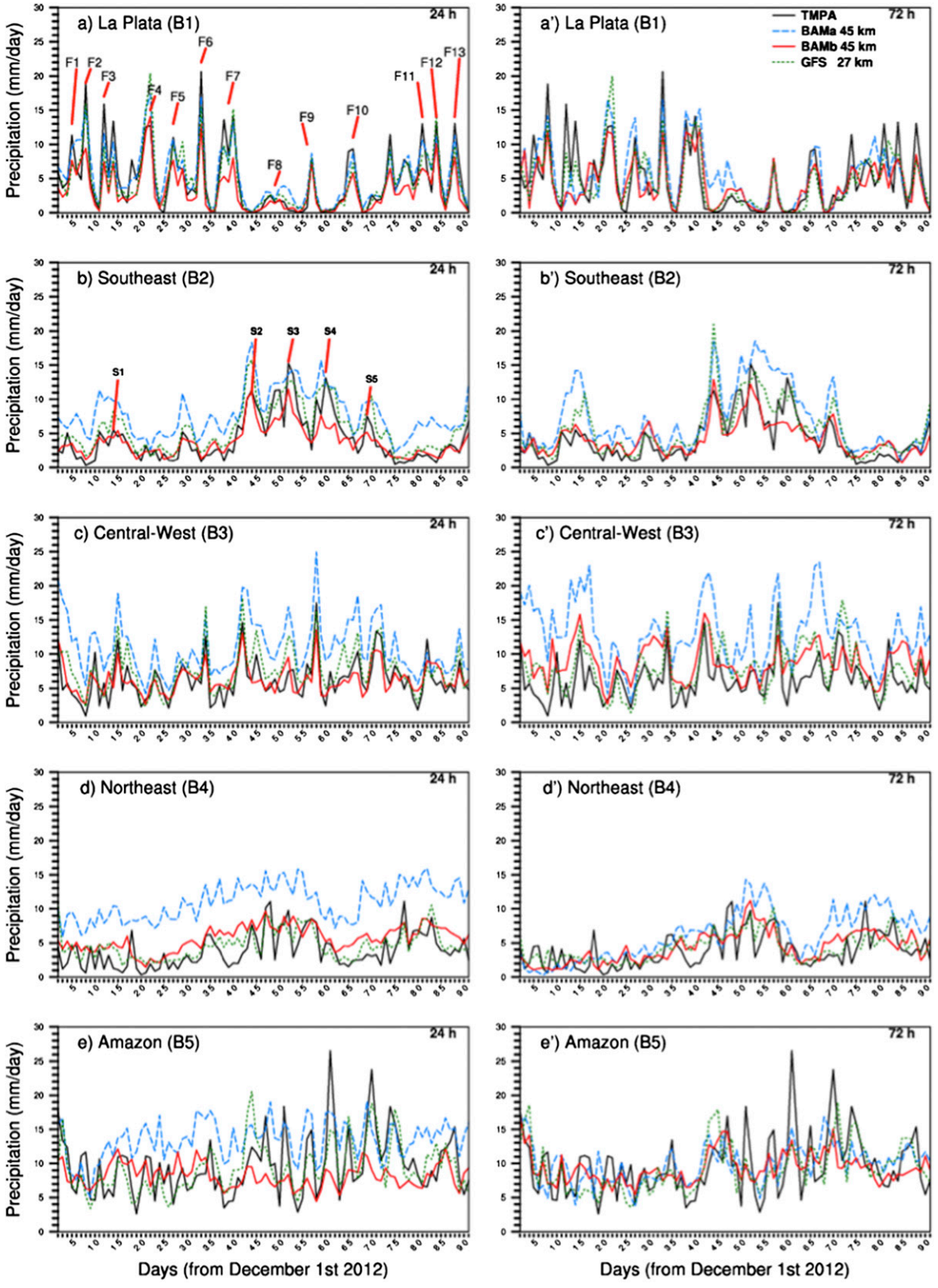

FIG. 9. Daily mean precipitation for the period 1 Dec 2012–28 Feb 2013 from (left) 24- and (right) 72-h forecasts for the areas defined in Fig. 8 from TMPA and three NWP models indicated in the panel. The letters F in (a) and S in (b) indicate cold fronts over La Plata and SACZ events over the Southeast region, respectively.

the region. In addition, this system indirectly affects the weather conditions over the South, Central-West, North, and Northeast regions of Brazil during DJF (Nogués-Paegle and Mo 1997). The SACZ's origin is not fully understood. However, preliminary modeling studies suggest that interactions between intense convection over the Amazon (as local forcing) with large-scale westerly winds (e.g., Figueroa et al. 1995) or frontal systems (e.g., Nieto Ferreira and Chao 2013) could be a possible cause of SACZ initiation. The dynamics of enhanced cloudiness and rainfall over cooler SSTs associated with the SACZ could be better explained by the use of coupled ocean–atmosphere models and direct observations (e.g., De Almeida et al. 2007).

Despite this fact, the five SACZ episodes identified during DJF 2012/13 (INPE/CPTEC 2012, 2013a,b), indicated by the letter S in Fig. 9b (from S1 to S5), were well predicted by BAMb as well as GFS, both their duration and intensity, 24- and 72 h in advance. Only in the S4 event, at the end of January (around day 60), was the precipitation amount underestimated by BAMb. A comparison of Figs. 9a and 9b shows an alternating pattern between the extreme precipitation events over the SACZ and La Plata regions, which is known as the South American dipole (Nogués-Paegle and Mo 1997).

When intense and persistent SACZ events occur over the Southeast (e.g., during January 2013, days 32–63), the precipitation over the La Plata region is drastically reduced. Conversely, when persistent intense precipitation occurs over La Plata (e.g., during December, days 1–31), the development of intense SACZ events is inhibited. This dipole-like precipitation structure on intraseasonal time scales between La Plata and southeastern Brazil, identified in many observational studies (e.g., Nogués-Paegle and Mo 1997), was reproduced well by the BAMb and GFS models, but overestimated by BAMa. While SACZ is a quasi-stationary system, the cold fronts arriving in this region from southern Brazil are transient perturbations, and the convective bands associated with them rapidly move northeastward (Lima et al. 2010). Most of the intense MCSs over this region are linked to these frontal incursions (Siqueira and Marques 2010). Also, these transient systems are responsible for maintaining or intensifying the convective activity in the SACZ, driving extreme precipitation events over this region.

Weather conditions over the Central-West region (B3) are also affected by squall lines, MCSs, the SACZ (mainly over the eastern part of this region), and frontal systems that occasionally reach the southern part of this region. The maximum seasonal precipitation over the Northeast (B4) occurs during March–May (MAM) and is linked to the Atlantic ITCZ's southernmost annual displacement (Moura and Shukla 1981; Nobre and Shukla 1996). However, weather conditions during DJF over the southern Northeast region are affected by convective activity associated with the upper-level cyclonic vortices, easterly waves, land–sea-breeze circulations (over coastal regions of B4), as well as occasional cold fronts and the SACZ reaching the southern part of this region (Chaves and Cavalcanti 2001). For instance, intense precipitation during the last 15 days of January (days 45–60) over the Northeast (Fig. 10d) was related to SACZ events (cf. Fig. 9d with Fig. 9b). Finally, weather conditions over the Amazon (area B5) during DJF are affected by convection organized by the SACZ (de Oliveira Vieira et al. 2013), MCSs, and squall lines, which originate along the northern coast of Brazil and propagate toward the Amazon, although these systems are more frequent during MAM (Cohen et al. 1995). The time series of TMPA precipitation estimated over the Amazon (Fig. 9e) shows a large degree of rainfall variability during the intense SACZ events over the Southeast (days 45–75), although the maximum precipitation values over the Amazon and SACZ regions do not occur simultaneously.

Similar to Fig. 4 (left), Fig. 10 (left) shows that the tendencies of the systematic errors (e.g., dry bias over the Amazon and La Plata) remain unchanged from 5- to 7-day forecasts. The RMSE (Fig. 10, right) shows that BAMb (at both 45- and 20-km resolution) performs much better than BAMa. Figure 11 depicts the GSS (right) along with FBS (left) at 72-h lead time for the areas defined in Fig. 8. A visual inspection of the frequency bias (Figs. 11a–e) shows that BAMa overpredicts moderate and heavy rainfall events over all regions, except over the Amazon, whereas BAMb at 45 km underpredicts rainfall. However, the predictions are improved (FBS values near 1) at high resolution, mainly over the Southeast. The GSS analysis shows that BAMb at 45 km is superior to BAMa for light and moderate rainfall over the Southeast and La Plata, whereas over other regions there are not clear differences. Over La Plata (Figs. 11a and 11a′), GFS performs much better than BAMb in terms of GSS; however, in the FBS analysis all models overpredict the occurrence of light and moderate rainfall. Major improvement is seen for BAMb (FBS and GSS) over the Southeast at high resolution for moderate and heavy rainfall compared to BAMa at 45 km (Figs. 11b and 11b′), even beyond the 72-h forecast (not shown). On the other hand, over the Amazon all models display lower Gilbert skill scores (Fig. 11e′). Improvement in QPF skill over this region will remain a great challenge.

A comparison of precipitation forecast statistics using the Taylor diagram (Fig. 12) and biases (Fig. 11, left) shows that BAMb is generally superior to BAMa for 1–7-day lead-time forecasts (smaller URMSE*, higher

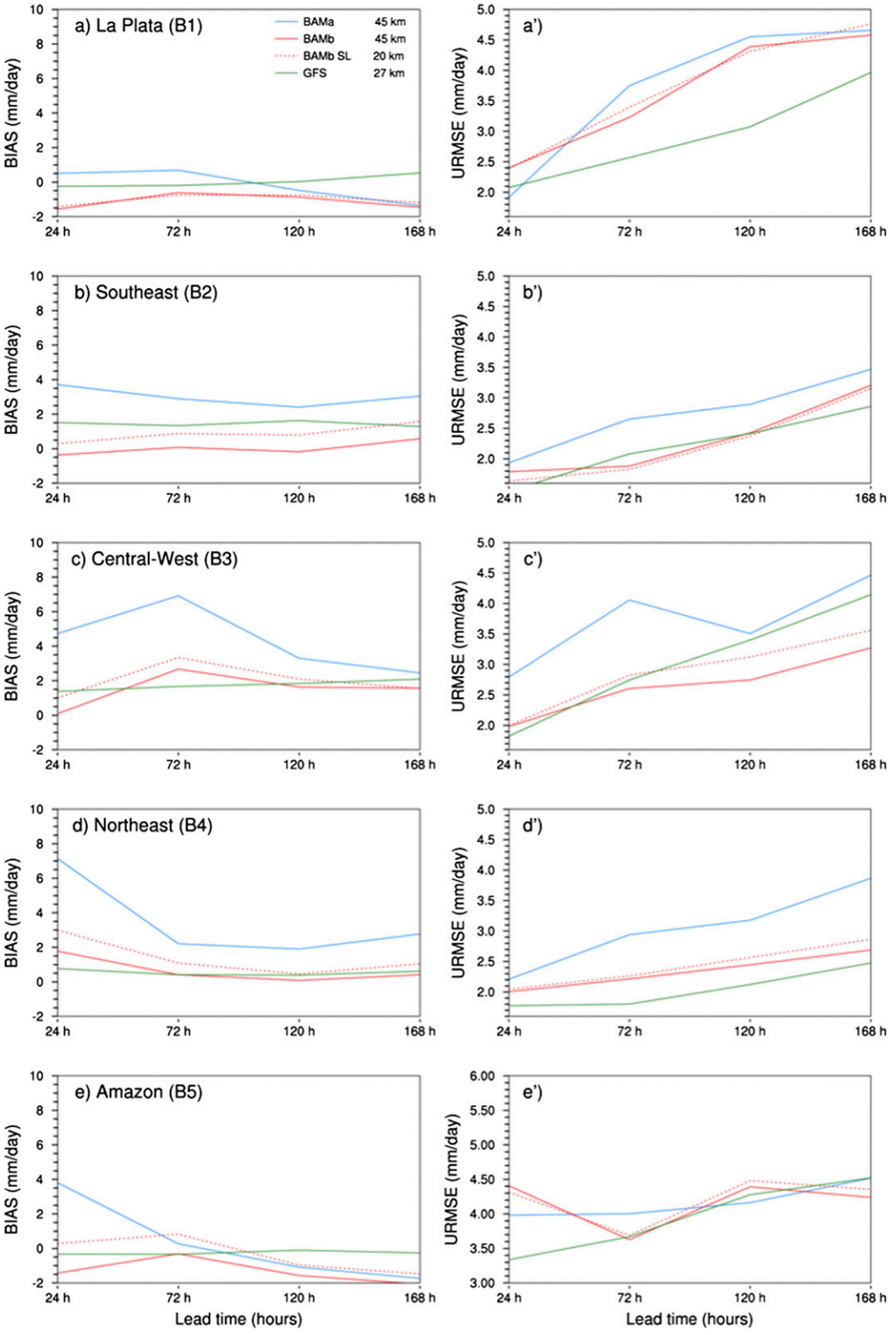

FIG. 10. As Fig. 5, but for the areas defined in Fig. 8.

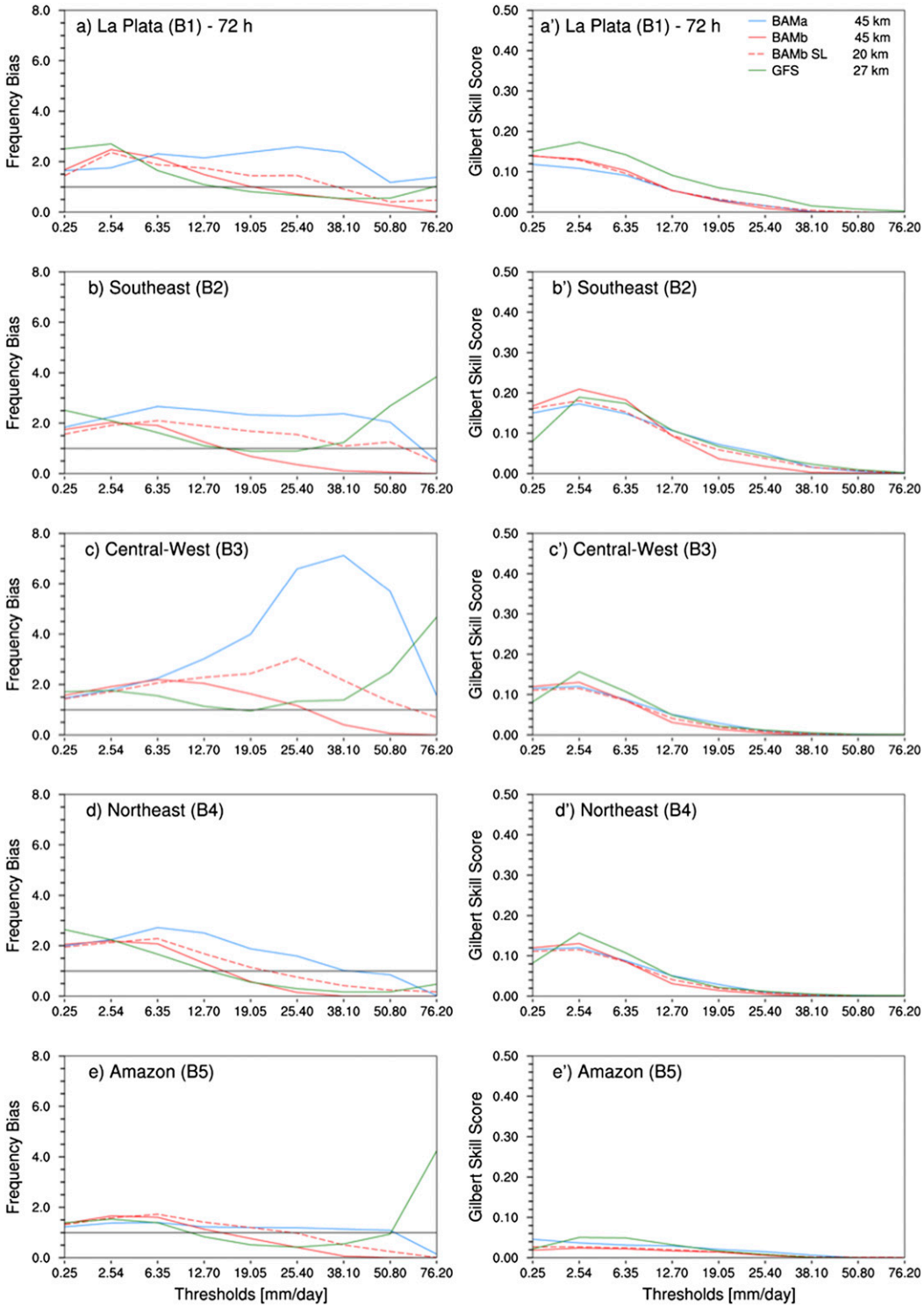

FIG. 11. As in Fig. 6, but for the areas defined in Fig. 8.

correlations, and smaller BIAS), except over the Amazon and La Plata, where they have similar performance. On the other hand, the comparisons between GFS and BAMb for 1–7-day forecasts at 45 km show similar URMSE* results and correlations over the La Plata, Southeast, Central-West, and Northeast regions, notwithstanding that the magnitude of the daily variability is better forecast by GFS. The performance of BAMb at

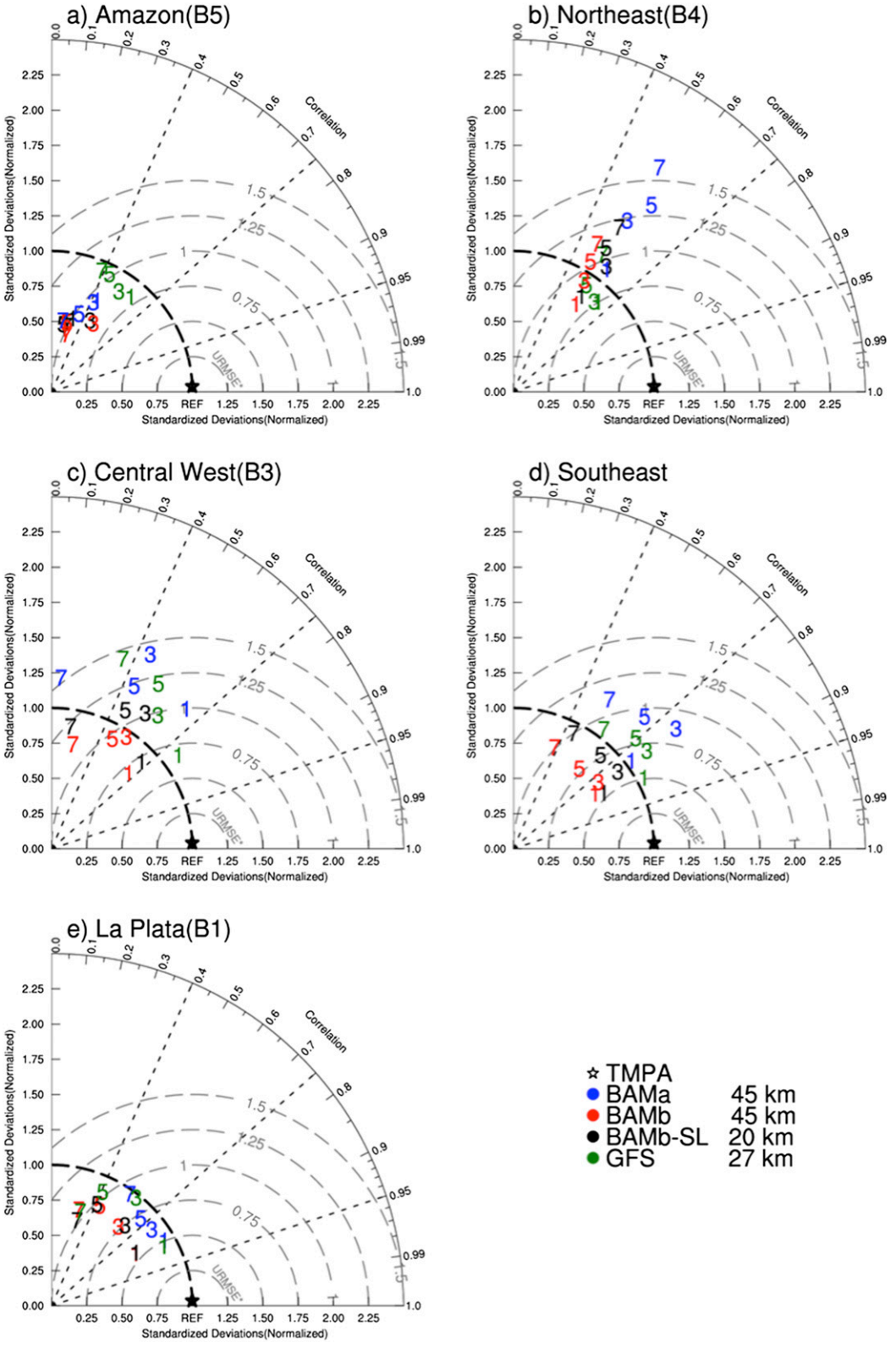

FIG. 12. As in Fig. 7, but for the areas defined in Fig. 8.

high resolution is similar to that at 45 km, except over the Southeast (B2) and Central-West (B3) (cf. red and black colored numbers in Fig. 12). Over these regions, one can see the improvement in the spread (standard deviation) of precipitation at high resolution, which is more noticeable over the Southeast. These results are consistent with the improvements in precipitation intensity, frequency bias, and Gilbert skill score for moderate and heavy rainfall over the Southeast, as discussed before.

In summary, the version of BAM with the GDM scheme outperforms the model with the GD scheme for QPFs over the regions depicted in Fig. 8. A comparison of results from low and high horizontal resolutions shows that the frequency bias as well as the Gilbert skill score is improved for moderate and heavy rainfall over the Southeast as the horizontal resolution increases (Figs. 11b and 11b′). The variance of precipitation over the Southeast also improves at high horizontal resolution (Fig. 12d). Finally, the systematic forecast errors in precipitation (dry or wet biases) over the regions shown in Fig. 8 remain practically unchanged from 5- to 7-day forecasts.

5. Summary and conclusions

The Brazilian Global Atmospheric Model (BAM) has been developed to overcome a number of shortcomings present in the previous CPTEC atmospheric global model (AGCM3) for the use over time scales ranging from days to seasons and horizontal resolution $O(10–100)$ km. BAM's dynamical core incorporates a monotonic two-time-level semi-Lagrangian scheme for the transport of moisture and microphysics prognostic variables and tracers, which are carried out completely on the model grid space. Some state-of-the-art physical parameterization schemes included in BAM are two convective parameterization schemes: GD and GDM among others (listed in Table 1).

The QPF skill from BAM with GD and GDM schemes and the sensitivity to increasing the horizontal resolutions are evaluated against the daily TRMM Multisatellite Precipitation Analysis (TMPA) over the tropical region for up to 7-day lead time during austral summer 2012/13. Three main results are summarized here. 1) The QPF skill was improved substantially with GDM in comparison to GD (smaller biases, smaller unbiased RMSE, higher correlations, improved frequency bias scores, and Gilbert skill scores) over all tropical regions evaluated (defined in Figs. 3a and 8). 2) The increase in horizontal resolution from 45 to 20 km, without any ad hoc tuning, enhances the intensity and variance of precipitation, and improves the frequency statistics of moderate and heavy rainfall events over the tropical continents with complex orography, such as Africa and South America, mainly over southeastern Brazil. Nevertheless, there was little difference between low and high resolutions over the oceans. 3) The systematic errors (dry or wet biases) seen during the first-day forecast over some tropical regions remained similar or increased with time (e.g., Central Africa, Amazon, and La Plata), whereas in other regions there were changes during the first 1–4-day forecasts. However, these errors remain virtually unchanged after 5-day forecasts.

From the first result stated above, we conclude that improving the convective parameterization in BAM (for which the Single-Column Model and Cloud Resolving Model were useful tools) is a key to improving the QPFs over the tropics. From the second result, we conclude that increasing the horizontal resolution in BAM from 45 to 20 km can benefit operational NWP over tropical continents with complex topography for predicting extreme rainfall events (e.g., during the SACZ events), mainly over southeastern Brazil.

Two caveats to this evaluation are pointed out. First, the quality of the forecast from BAM can be affected by the use of initial conditions produced from other data assimilation systems (i.e., NCEP/GFS). However, using the same initial condition as the NCEP/GFS forecast system has made the model comparison more robust. Second, the period of evaluation, 7-day forecasts for 3 months, might not be enough for drawing conclusions regarding the performance of the new model for precipitation forecasts. Further, for QPFs and other variables (e.g., wind, temperature, radiation, clouds, etc.), evaluations for different seasons of the year and for different years using CPTEC's data assimilation system are necessary. Yet, the present exercise served to show relevant improvements in the precipitation forecasts by the new convective scheme GDM compared to the original GD scheme, as well as to explore the benefits of using the 20-km horizontal resolution of the CPTEC global model in operational NWP. Based on this study, the semi-Lagrangian TQ666L96 (≈20 km and 96 vertical levels) BAM became operational on 1 January 2016 (after being used in experimental mode for 1 yr), replacing the previous operational TQ299L64 (≈45 km and 64 vertical levels).

Although tropical precipitation forecasts have been improved with the BAM, especially over southeastern Brazil, the total rainfall and its variance over the Amazon and La Plata regions are still underestimated. In a forthcoming paper, we will show that similar systematic errors are found in BAM climate simulations with the prescribed sea surface temperature. Improving the precipitation forecast over these regions remains a challenge for the future development of BAM.

TABLE A1. Brief overview of mass fluxes and parameters used in the GDM ensemble scheme. In this scheme six different closures (three perturbations for the Grell closure and three perturbations for the CAPE-based closure) from the dynamic control are allowed to interact with nine members from the static control (three efficiencies and three cap strengths), giving a total of 54 subgrid members.

Dynamic and static control	Definition of the type of closures in dynamic control and parameters in static control	No. of variations	Mass flux (dynamic control) or parameters (static control)
Dynamic control	Grell closure—assume AS quasi-equilibrium between large-scale forcing (LS) and convection (Grell 1993)	3	$m_b = -\frac{1}{K}\left(\frac{\partial A}{\partial t}\right)_{\text{LS}}$ $A = \int_{z_b}^{z_t} \eta(z) B(z)\, dz$
Dynamic control	CAPE-based closure—assumes that quasi-equilibrium exists between convection and the large-scale process in the free troposphere (Zhang 2002, 2009); note that CAPE_{env} is similar to the work function definition, but without weighing by a normalized mass flux profile η and that the buoyancy force B can be calculated with and without dilution	3	$m_b = -\frac{1}{K}\left(\frac{\partial \text{CAPE}_{\text{env}}}{\partial t}\right)_{\text{LS}}$ $\text{CAPE}_{\text{env}} = \int_{z_b}^{z_t} B(z)\, dz$
Static control feedback	Precipitation efficiency f perturbations—the convective rainfall R is defined as a function of precipitation efficiency f and integrated condensate in the updraft I, which depends on the total water that is rained out S_u and m_a (Grell and Dévényi 2002)	3	$R = fIm_a$, $I(\lambda) = \int_{z_b}^{z_t} n_u(\lambda, z) S_u\, dz$ $f = (0.25, 0.5, 0.75)$
Static control feedback	Maximum depth of capping (CapMax) perturbations—scheme does not allow convection until the lifting required for parcels to reach their level of free convection becomes less than the specified CapMax (25 mb < CapMax)	3	CapMax = (60, 90, 120)

Acknowledgments. The authors acknowledge NCEP for providing the analysis dataset used in this study as well as forecasts from the NCEP/GFS model. The authors thank Dr. Fedor Mesinger and the reviewers for a critical review of this manuscript and constructive comments. This research was partially funded by the following Brazilian agencies: FAPESP, CNPq, and the Brazilian Research Network on Global Climate Change FINEP/Rede CLIMA (Grant 01.13.0353-00).

APPENDIX

The Modified Grell and Dévényi Convective Scheme (GDM)

We have found in our experiments that by using the GD scheme in BAM (either ensemble and individual closures) the rainfall over the ITCZs, Africa, and South America, mainly over the Andes, are systematically overestimated (Fig. 1c), which is discussed in section 3. The large wet biases over the Andes have been investigated using the BAM Single-Column Model (BAM-SCM) and the System of Atmospheric Modeling (SAM, version 6.8.2) Cloud Resolving Model (CRM) developed by Khairoutdinov and Randall (2003). Based on these results, the original GD scheme described above was modified considering two important aspects: 1) AS, KF_type, Kuo_type, and Omega closures were excluded and instead an undiluted convective available potential energy (CAPE) based closure described in Zhang (2002) and Zhang (2009) was included, and 2) the original entrainment rate scheme $\varepsilon = 0.2/R$ was replaced by a new simplified scheme $\varepsilon = \epsilon_0/[z(k) - z(k_b - 1)]$, where R is the radius of the rising plume (12 000 m), $z(k)$

is the height at model level k, $z(k_b)$ is the height at cloud-base level $[z(k) > z(k_b - 1)]$, and ϵ_0 is a tunable parameter of $O(10^{-2})$. In Table A1, we summarized the closures and parameters used in this scheme, which is referred here as the GDM scheme. Its performance in global NWP compared to the GD scheme (e.g., Figs. 1d and 1c) is discussed in section 4. The details of this modified scheme, and its impact on the improvement of the precipitation simulation over the Andes, will be reported upon in a separate article. The remainder of this section describes how the GD scheme was modified using SAM and BAM-SCM, and discusses the main reason for the improvement in the simulated precipitation over the Andes with the modified scheme.

The averaged large-scale forcing (temperature and humidity advections, pressure, wind, and vertical velocity) used for the CRM [1 km × 1 km horizontal grid spacing, 144 × 144 grid points, and with the two-moment Morrison microphysics scheme; Morrison et al. (2009)] and SCM simulations (BAM-SCM with parameterization physics described in Table 1) were calculated from the 6-hourly NCEP/GFS analysis for the period 1–30 January 2013, over a 5° × 5° (latitude–longitude) area centered approximately over the Peru–Bolivian Plateau (16.5°S, 69°W). First, the precipitation from CRM was compared with the daily precipitation estimated by satellite (TMPA, database details in section 3) then results from BAM-SCM were compared with the CRM simulations.

The CRM simulates the precipitation reasonably well in comparison to TMPA with maximum values around 10 mm day^{-1}, although uncertainties exist in the precipitation and large-scale forcing results estimated over complex topography. The results from BAM-SCM reveal (figure not shown) that the daily precipitation patterns and intensity are poorly simulated when using the original GD scheme in comparison to CRM and observations; in contrast, results from GDM are similar to those of CRM. Overall, the GD scheme overestimates TMPA by approximately threefold. We found that results were much improved when we only used G1 and the Zhang scheme as closures, so all other closures were excluded in GDM. The averaged (January 2013) mass-flux profile from CRM/SAM, BAM-SCM with the GD scheme, and 1D with the GDM scheme reveals (figure not shown) that the mass-flux from GD is almost 3 times higher than from CRM (maximum value from CRM is around 0.02 kg m^{-2} s^{-2}), whereas that from GDM, at least in the first 6 km above cloud base, is close to the CRM results. The improvement in the GDM simulation is attributed mainly to 1) the exclusion of some closures, 2) the addition of the CAPE-based closure, and 3) the inclusion of the new simple entrainment scheme with ϵ_0 tuned using CRM/SAM results.

REFERENCES

Alpert, J. C., M. Kanamitsu, P. M. Caplan, J. G. Sela, G. H. White, and E. Kalnay, 1988: Mountain induced gravity wave drag parameterization in the NMC medium-range model. Preprints, *Eighth Conf. on Numerical Weather Prediction*, Baltimore, MD, Amer. Meteor. Soc., 726–733.

Arakawa, A., and W. H. Schubert, 1974: Interaction of a cumulus cloud ensemble with the large-scale environment, Part I. *J. Atmos. Sci.*, **31**, 674–701, doi:10.1175/1520-0469(1974)031<0674:IOACCE>2.0.CO;2.

Arraut, J. M., and H. M. J. Barbosa, 2009: Large-scale features associated with strong frontogenesis in equivalent potential temperature in the South American subtropics east of the Andes. *Adv. Geosci.*, **22**, 73–78, doi:10.5194/adgeo-22-73-2009.

——, and P. Satyamurty, 2009: Precipitation and water vapor transport in the Southern Hemisphere with emphasis on the South American region. *J. Appl. Meteor. Climatol.*, **48**, 1902–1912, doi:10.1175/2009JAMC2030.1.

Barbosa, H. M. J., T. A. Tarasova, and I. F. A. Cavalcanti, 2008: Impacts of a new solar radiation parameterization on the CPTEC AGCM climatological features. *J. Appl. Meteor. Climatol.*, **47**, 1377–1392, doi:10.1175/2007JAMC1760.1.

Berbery, E. H., and V. R. Barros, 2002: The hydrologic cycle of the La Plata basin in South America. *J. Hydrometeor.*, **3**, 630–645, doi:10.1175/1525-7541(2002)003<0630:THCOTL>2.0.CO;2.

Boers, N., B. Bookhagen, H. M. J. Barbosa, N. Marwan, J. Kurths, and J. Marengo, 2014: Prediction of extreme floods in the eastern central Andes based on a complex network approach. *Nat. Commun.*, **5**, 5199, doi:10.1038/ncomms6199.

——, H. M. J. Barbosa, B. Bookhagen, J. A. Marengo, N. Marwan, and J. Kurths, 2015: Propagation of strong rainfall events from southeastern South America to the central Andes. *J. Climate*, **28**, 7641–7658, doi:10.1175/JCLI-D-15-0137.1.

Brown, J. M., 1979: Mesoscale unsaturated downdrafts driven by rainfall evaporation: A numerical study. *J. Atmos. Sci.*, **36**, 313–338, doi:10.1175/1520-0469(1979)036<0313:MUDDBR>2.0.CO;2.

Cavalcanti, I. F. A., and Coauthors, 2002: Global climatological features in a simulation using the CPTEC–COLA AGCM. *J. Climate*, **15**, 2965–2988, doi:10.1175/1520-0442(2002)015<2965:GCFIAS>2.0.CO;2.

Chaves, R. R., and I. F. A. Cavalcanti, 2001: Atmospheric circulation features associated with rainfall variability over southern Northeast Brazil. *Mon. Wea. Rev.*, **129**, 2614–2626, doi:10.1175/1520-0493(2001)129<2614:ACFAWR>2.0.CO;2.

Chen, Y., E. E. Ebert, K. J. E. Walsh, and N. E. Davidson, 2013: Evaluation of TMPA 3B42 daily precipitation estimates of tropical cyclone rainfall over Australia. *J. Geophys. Res. Atmos.*, **118**, 11 966–11 978, doi:10.1002/2013JD020319.

Chou, M. D., and M. J. Suarez, 1999: A solar radiation parameterization for atmospheric studies. NASA Tech. Rep. NASA/TM-1999-10460, Vol. 15, 40 pp. [Available online at https://gmao.gsfc.nasa.gov/pubs/docs/Chou136.pdf.]

Cohen, J. C. P., M. A. F. Silva Dias, and C. A. Nobre, 1995: Environmental conditions associated with Amazonian squall lines: A case study. *Mon. Wea. Rev.*, **123**, 3163–3174, doi:10.1175/1520-0493(1995)123<3163:ECAWAS>2.0.CO;2.

Costa, M. H., and G. F. Pires, 2010: Effects of Amazon and central Brazil deforestation scenarios on the duration of the dry season

in the arc of deforestation. *Int. J. Climatol.*, **30**, 1970–1979, doi:10.1002/joc.2048.

——, S. N. M. Yanagi, P. J. Oliveira, A. Ribeiro, and E. J. P. Rocha, 2007: Climate change in Amazonia caused by soybean cropland expansion, as compared to caused by pasture land expansion. *Geophys. Res. Lett.*, **34**, L07706, doi:10.1029/2007GL029271.

Cunha, A. P. M. A., R. C. S. Avalá, G. Sampaio, M. H. Shimizu, and M. H. Costa, 2013: Calibration and validation of the Integrated Biosphere Simulator (IBIS) for a Brazilian semiarid region. *J. Appl. Meteor. Climatol.*, **52**, 2753–2770, doi:10.1175/JAMC-D-12-0190.1.

Cunningham, C., J. P. Bonatti, and M. Ferreira, 2014: Assessing improved CPTEC probabilistic forecasts on medium-range timescale. *Meteor. Appl.*, **22**, 378–384, doi:10.1002/met.1464.

De Almeida, R. F., P. Nobre, R. J. Haarsma, and E. J. D. Campos, 2007: Negative ocean-atmosphere feedback in the South Atlantic Convergence Zone. *Geophys. Res. Lett.*, **34**, L18809, doi:10.1029/2007GL030401.

Dee, D. P., and Coauthors, 2011: The ERA-Interim reanalysis: Configuration and performance of the data assimilation system. *Quart. J. Roy. Meteor. Soc.*, **137**, 553–597, doi:10.1002/qj.828.

de Oliveira Vieira, S., P. Satyamurty, and R. V. Andreoli, 2013: On the South Atlantic Convergence Zone affecting southern Amazonia in austral summer. *Atmos. Sci. Lett.*, **14**, 1–6, doi:10.1002/asl2.401.

Figueroa, S. N., P. Satyamurty, and P. L. Silva Dias, 1995: Simulations of the summer circulation over the South American region with an eta coordinate model. *J. Atmos. Sci.*, **52**, 1573–1584, doi:10.1175/1520-0469(1995)052<1573:SOTSCO>2.0.CO;2.

——, T. Tarasova, H. M. J. Barbosa, J. P. Bonatti, and P. L. Silvia Dias, 2006: The impact of cumulus and radiation parameterization schemes on Southern Hemisphere summer climate simulated by CPTEC atmospheric general circulation model. *Proc. Eighth Int. Conf. on Southern Hemisphere Meteorology and Oceanography*, Foz do Iguaçu, Brazil, INPE, 1037–1040. [Available online at http://apcling.org/programs/Foz2006SilvioEtAl.pdf.]

Foley, J. A., I. C. Prentice, N. Ramankutty, S. Levis, D. Pollard, S. Sitch, and A. Haxeltine, 1996: An integrated biosphere model of land surface processes, terrestrial carbon balance, and vegetation dynamics. *Global Biogeochem. Cycles*, **10**, 603–628, doi:10.1029/96GB02692.

Fritsch, J. M., and R. E. Carbone, 2004: Improving quantitative precipitation forecasts in the warm season: A USWRP research and development strategy. *Bull. Amer. Meteor. Soc.*, **85**, 955–965, doi:10.1175/BAMS-85-7-955.

Garreaud, R. D., and J. M. Wallace, 1998: Summertime incursions of midlatitude air into subtropical and tropical South America. *Mon. Wea. Rev.*, **126**, 2713–2733, doi:10.1175/1520-0493(1998)126<2713:SIOMAI>2.0.CO;2.

Grell, G., 1993: Prognostic evaluation of assumptions used by cumulus parameterizations. *Mon. Wea. Rev.*, **121**, 764–787, doi:10.1175/1520-0493(1993)121<0764:PEOAUB>2.0.CO;2.

——, and D. Dévényi, 2002: A generalized approach to parameterizing convection combining ensemble and data assimilation techniques. *Geophys. Res. Lett.*, **29**, doi:10.1029/2002GL015311.

Grose, M. R., and Coauthors, 2014: Assessment of the CMIP5 global climate model simulations of the western tropical Pacific climate system and comparison to CMIP3. *Int. J. Climatol.*, **34**, 3382–3399, doi:10.1002/joc.3916.

Gulizia, C., and I. Camilloni, 2014: Comparative analysis of the ability of a set of CMIP3 and CMIP5 global climate models to represent precipitation in South America. *Int. J. Climatol.*, **35**, 583–595, doi:10.1002/joc.4005.

Hirota, N., and Y. N. Takayabu, 2013: Reproducibility of precipitation distribution over the tropical oceans in CMIP5 multi-climate models compared to CMIP3. *Climate Dyn.*, **41**, 2909–2920, doi:10.1007/s00382-013-1839-0.

Huffman, G. J., R. F. Adler, D. T. Bolvin, and G. Gu, 2009: Improving the global precipitation record: GPCP version 2.1. *Geophys. Res. Lett.*, **36**, L17808, doi:10.1029/2009GL040000.

——, ——, ——, and E. J. Nelkin, 2010: The TRMM Multi-satellite Precipitation Analysis (TMPA). *Satellite Applications for Surface Hydrology*, M. Gebremichael and F. Hossain, Eds., Springer, 3–22, doi:10.1007/978-90-481-2915-7_1.

Iacono, M., J. Delamere, E. Mlawer, M. Shephard, S. Clough, and W. Collins, 2008: Radiative forcing by long-lived greenhouse gases: Calculations with the AER radiative transfer models. *J. Geophys. Res.*, **113**, D13103, doi:10.1029/2008JD009944.

INPE/CPTEC, 2012: Climanálise: Boletim de Monitoramento e Análise Climática. Vol. 27, No. 12, INPE/CPTEC, 42 pp. [Available online at http://climanalise.cptec.inpe.br/~rclimanl/boletim/pdf/pdf12/dez12.pdf.]

——, 2013a: Climanálise: Boletim de Monitoramento e Análise Climática. Vol. 28, No. 1, CPTEC/INPE, 44 pp. [Available online at http://climanalise.cptec.inpe.br/~rclimanl/boletim/pdf/pdf13/jan13.pdf.]

——, 2013b: Climanálise: Boletim de Monitoramento e Análise Climática. Vol. 28, No. 2, CPTEC/INPE, 45 pp. [Available online at http://climanalise.cptec.inpe.br/~rclimanl/boletim/pdf/pdf13/fev13.pdf.]

Jones, C., and L. M. V. Carvalho, 2013: Climate change in the South American monsoon system: Present climate and CMIP5 projections. *J. Climate*, **26**, 6660–6678, doi:10.1175/JCLI-D-12-00412.1.

Kain, J. S., and J. M. Fritsch, 1992: The role of the convective "trigger function" in numerical forecasts of mesoscale convective systems. *Meteor. Atmos. Phys.*, **49**, 93–106, doi:10.1007/BF01025402.

Khairoutdinov, M. F., and D. A. Randall, 2003: Cloud-resolving modeling of the ARM summer 1997 IOP: Model formulation, results, uncertainties, and sensitivities. *J. Atmos. Sci.*, **60**, 607–625, doi:10.1175/1520-0469(2003)060<0607:CRMOTA>2.0.CO;2.

Kitade, T., 1983: Nonlinear normal mode initialization with physics. *Mon. Wea. Rev.*, **111**, 2194–2213, doi:10.1175/1520-0493(1983)111<2194:NNMIWP>2.0.CO;2.

Krishnamurti, T. N., S. Low-Nam, and R. Pasch, 1983: Cumulus parameterizations and rainfall rates II. *Mon. Wea. Rev.*, **111**, 815–828, doi:10.1175/1520-0493(1983)111<0815:CPARRI>2.0.CO;2.

Kubota, P. Y., 2012: Variability of storage energy in the soil-canopy system and its impact on the definition of precipitation standard in South America (in Portuguese with abstract in English). Ph.D. thesis, Instituto Nacional de Pesquisas Espaciais (INPE), São José dos Campos, Brazil, 285 pp.

Kucharik, C. J., and Coauthors, 2000: Testing the performance of a dynamic global ecosystem model: Water balance, carbon balance, and vegetation structure. *Global Biogeochem. Cycles*, **14**, 795–826, doi:10.1029/1999GB001138.

Lima, K. C., P. Satyamurty, and J. P. R. Fernández, 2010: Large-scale atmospheric conditions associated with heavy rainfall episodes in Southeast Brazil. *Theor. Appl. Climatol.*, **101**, 121–135, doi:10.1007/s00704-009-0207-9.

Ma, H.-Y., and Coauthors, 2014: On the correspondence between mean forecast errors and climate errors in CMIP5 models. *J. Climate*, **27**, 1781–1798, doi:10.1175/JCLI-D-13-00474.1.

Machenhauer, B., 1977: On the dynamics of gravity oscillations in a shallow water model with applications to normal mode initialization. *Contrib. Atmos. Phys.*, **50**, 253–271.

Martin, G. M., D. W. Johnson, and A. Spice, 1994: The measurement and parameterization of effective radius of droplets in warm stratocumulus clouds. *J. Atmos. Sci.*, **51**, 1823–1842, doi:10.1175/1520-0469(1994)051<1823:TMAPOE>2.0.CO;2.

Mehran, A., A. Agha Kouchak, and T. J. Phillips, 2014: Evaluation of CMIP5 continental precipitation simulations relative to satellite-based gauge-adjusted observations. *J. Geophys. Res. Atmos.*, **119**, 1695–1707, doi:10.1002/2013JD021152.

Mellor, G. L., and T. Yamada, 1982: Development of a turbulence closure model for geophysical fluid problems. *Rev. Geophys. Space Phys.*, **20**, 851–875, doi:10.1029/RG020i004p00851.

Mesinger, F., 2008: Bias adjusted precipitation threat scores. *Adv. Geosci.*, **16**, 137–142, doi:10.5194/adgeo-16-137-2008.

——, and T. L. Black, 1992: On the impact on forecast accuracy of the step-mountain (eta) vs. sigma coordinate. *Meteor. Atmos. Phys.*, **50**, 47–60, doi:10.1007/BF01025504.

Mlawer, E. J., S. J. Taubman, P. D. Brown, M. J. Iacono, and S. A. Clough, 1997: Radiative transfer for inhomogeneous atmospheres: RRTM, a validated correlated-k model for the longwave. *J. Geophys. Res.*, **102**, 16 663–16 682, doi:10.1029/97JD00237.

Morrison, G., J. A. Curry, and V. I. Khvorostyanov, 2005: A new double-moment microphysics parameterization for application in cloud and climate models. Part I: Description. *J. Atmos. Sci.*, **62**, 1665–1677, doi:10.1175/JAS3446.1.

——, G. Thompson, and V. Tatarskii, 2009: Impact of cloud microphysics on the development of trailing stratiform precipitation in a simulated squall line: Comparison of one- and two-moment schemes. *Mon. Wea. Rev.*, **137**, 991–1007, doi:10.1175/2008MWR2556.1.

Moura, A. D., and J. Shukla, 1981: On the dynamics of droughts in Northeast Brazil: Observations, theory and numerical experiments with a general circulation model. *J. Atmos. Sci.*, **38**, 2653–2675, doi:10.1175/1520-0469(1981)038<2653:OTDODI>2.0.CO;2.

Murphy, A. H., 1988: Skill scores based on the mean square error and their relationships to the correlation coefficient. *Mon. Wea. Rev.*, **116**, 2417–2424, doi:10.1175/1520-0493(1988)116<2417:SSBOTM>2.0.CO;2.

Neale, R. B., and Coauthors, 2012: Description of the NCAR Community Atmosphere Model (CAM 5.0). NCAR Tech. Note NCAR/TN-486+STR, 274 pp. [Available online at http://www.cesm.ucar.edu/models/cesm1.0/cam/docs/description/cam5_desc.pdf.]

Nieto Ferreira, R., and W. C. Chao, 2013: 2013: Aqua-planet simulations of the formation of South Atlantic convergence zone. *Int. J. Climatol.*, **33**, 615–628, doi:10.1002/joc.3457.

Nobre, P., and J. Shukla, 1996: Variations of sea surface temperature, wind stress, and rainfall over the tropical Atlantic and South America. *J. Climate*, **9**, 2464–2479, doi:10.1175/1520-0442(1996)009<2464:VOSSTW>2.0.CO;2.

——, M. Malagutti, D. F. Urbano, R. A. F. de Almeida, and E. Giarolla, 2009: Amazon deforestation and climate change in a coupled model simulation. *J. Climate*, **22**, 5686–5697, doi:10.1175/2009JCLI2757.1.

——, and Coauthors, 2013: Climate simulation and change in the Brazilian climate model. *J. Climate*, **26**, 6716–6732, doi:10.1175/JCLI-D-12-00580.1.

Nogués-Paegle, J., and K. C. Mo, 1997: Alternating wet and dry conditions over South America during summer. *Mon. Wea. Rev.*, **125**, 279–291, doi:10.1175/1520-0493(1997)125<0279:AWADCO>2.0.CO;2.

Ochoa, A., L. Pineda, P. Willems, and P. Crespo, 2014: Evaluation of TRMM 3B42 (TMPA) precipitation estimates and WRF retrospective precipitation simulation over the Pacific-Andean basin into Ecuador and Peru. *Hydrol. Earth Syst. Sci.*, **11**, 411–449, doi:10.5194/hessd-11-411-2014.

Panetta, J., S. R. Barros, J. P. Bonatti, S. S. Tomita, and P. Y. Kubota, 2007: Computational cost of CPTEC AGCM. *Proc. 12th Workshop on Use of High Performance Computing in Meteorology*, Reading, United Kingdom, ECMWF, 65–83.

Park, S., and C. S. Bretherton, 2009: The University of Washington shallow convection and moist turbulence schemes and their impact on climate simulations with the Community Atmosphere Model. *J. Climate*, **22**, 3449–3469, doi:10.1175/2008JCLI2557.1.

Pincus, R., H. W. Barker, and J.-J. Morcrette, 2003: A fast, flexible, approximate technique for computing radiative transfer in inhomogeneous cloud fields. *J. Geophys. Res.*, **108**, 4376, doi:10.1029/2002JD003322.

Rasch, P. J., and J. E. Kristjansson, 1998: A comparison of the CCM3 model climate using diagnosed and predicted condensate parameterizations. *J. Climate*, **11**, 1587–1614, doi:10.1175/1520-0442(1998)011<1587:ACOTCM>2.0.CO;2.

Rasmussen, K. L., and R. A. Houze Jr., 2016: Convective initiation near the Andes in subtropical South America. *Mon. Wea. Rev.*, **144**, 2351–2374, doi:10.1175/MWR-D-15-0058.1.

——, M. M. Chaplin, M. D. Zuluaga, and R. A. Houze Jr., 2016: Contribution of extreme convective storms to rainfall in South America. *J. Hydrometeor.*, **17**, 353–367, doi:10.1175/JHM-D-15-0067.1.

Reisner, J., R. M. Rasmussen, and R. T. Bruintjes, 1998: Explicit forecasting of supercooled liquid water in winter storms using the MM5 mesoscale model. *Quart. J. Roy. Meteor. Soc.*, **124**, 1071–1107, doi:10.1002/qj.49712454804.

Romatschke, U., and R. A. Houze Jr., 2010: Extreme summer convection in South America. *J. Climate*, **23**, 3761–3791, doi:10.1175/2010JCLI3465.1.

Rozante, J. R., and I. F. A. Cavalcanti, 2008: Regional Eta model experiments: SALLJEX and MCS development. *J. Geophys. Res.*, **113**, D17106, doi:10.1029/2007JD009566.

Salio, P., M. Nicolini, and E. J. Zipser, 2007: Mesoscale convective systems over southeastern South America and their relationship with the South American low-level jet. *Mon. Wea. Rev.*, **135**, 1290–1309, doi:10.1175/MWR3305.1.

Sato, N., P. J. Sellers, D. A. Randall, E. K. Schneider, J. Shukla, J. L. Kinter III, Y. T. Hou, and E. Albertazzi, 1989: Effects of implementing the Simple Biosphere Model in a general circulation model. *J. Atmos. Sci.*, **46**, 2757–2782, doi:10.1175/1520-0469(1989)046<2757:EOITSB>2.0.CO;2.

Siqueira, J. R., and V. S. Marques, 2010: Structural characteristics of mesoscale convective systems over southeast Brazil related to cold frontal and non-frontal incursions. *Aust. Meteor. Oceanogr. J.*, **60**, 49–62.

Stern, H., 2008: The accuracy of forecasts for Melbourne, Australia. *Meteor. Appl.*, **15**, 65–71, doi:10.1002/met.67.

——, and N. E. Davidson, 2015: Trends in the skill of weather prediction at lead times of 1–14 days. *Quart. J. Roy. Meteor. Soc.*, **141**, 2726–2736, doi:10.1002/qj.2559.

Tarasova, T., and B. Fomin, 2000: Solar radiation absorption due to water vapor: Advanced broadband parameterizations. *J. Appl. Meteor.*, **39**, 1947–1951, doi:10.1175/1520-0450(2000)039<1947:SRADTW>2.0.CO;2.

Taylor, K. E., 2001: Summarizing multiple aspects of model performance in a single diagram. *J. Geophys. Res.*, **106**, 7183–7192, doi:10.1029/2000JD900719.

Tiedtke, M., 1983: The sensitivity of the time-mean large-scale flow to cumulus convection in the ECMWF model. *Proc. Workshop on Convection in Large-Scale Models*, Reading, United Kingdom, ECMWF, 297–316.

Webster, S., A. R. Brown, D. R. Cameron, and C. P. Jones, 2003: Improvements to the representation of orography in the Met Office United Model. *Quart. J. Roy. Meteor. Soc.*, **129**, 1989–2010, doi:10.1256/qj.02.133.

WMO, 2009: Recommendations for the verification and intercomparison of QPFs and PQPFs from operational NWP models: Revision 2. WMO/TD-No.1485, WWRP 2009-1, 37 pp. [Available online at http://www.wmo.int/pages/prog/arep/wwrp/new/documents/WWRP2009-1_web_CD.pdf.]

Xie, S., H.-Y. Ma, J. S. Boyle, S. A. Klein, and Y. Zhang, 2012: On the correspondence between short- and long-time-scale systematic errors in CAM4/CAM5 for the Year of Tropical Convection. *J. Climate*, **25**, 7937–7955, doi:10.1175/JCLI-D-12-00134.1.

Xue, Y., P. J. Sellers, J. L. Kinter, and J. Shukla, 1991: A simplified biosphere model for global climate studies. *J. Climate*, **4**, 345–364, doi:10.1175/1520-0442(1991)004<0345:ASBMFG>2.0.CO;2.

Yin, L., F. Fu, E. Shevliakova, and R. E. Dickinson, 2013: How well can CMIP5 simulate precipitation and its controlling processes over tropical South America? *Climate Dyn.*, **41**, 3127–3143, doi:10.1007/s00382-012-1582-y.

Zeng, X., M. Zhao, and R. E. Dickinson, 1998: Intercomparison of bulk aerodynamical algorithms for the computation of sea surface fluxes using TOGA COARE and TAO data. *J. Climate*, **11**, 2628–2644, doi:10.1175/1520-0442(1998)011<2628:IOBAAF>2.0.CO;2.

Zhang, G. J., 2002: Convective quasi-equilibrium in midlatitude continental environment and its effect on convective parameterization. *J. Geophys. Res.*, **107**, doi:10.1029/2001JD001005.

——, 2009: Effects of entrainment on convective available potential energy and closure assumptions in convection parameterization. *J. Geophys. Res.*, **114**, D07109, doi:10.1029/2008JD010976.

Zhu, H., M. C. Wheeler, A. H. Sobel, and D. Hudson, 2014: Seamless precipitation prediction skill in the tropics and extratropics from a global model. *Mon. Wea. Rev.*, **142**, 1556–1569, doi:10.1175/MWR-D-13-00222.1.